Experimental and numerical study on the mechanical properties of adhesive joints under impact loads using Ls-Dyna.

Politecnico di Torino

Master of Science in Mechanical Engineering

A.A. 2020/2021

Student:
Muhammad Akif Akram Malik

Advisor:
Prof. Luca Goglio

Co-Advisors:
Boursier Carlo Niutta
Ciardiello Raffaele
Fiumarella Dario

Department of Mechanical and Aerospace Engineering
Politecnico di Torino

Table of Contents

List of Figures

List of Tables

List of Acronyms

PMS Painted metal substrate

CHZ Cohesive Zone Modelling

SHPB Split Hopkinson Pressure Bar

DCB Double Cantilever Beam

DIC Digital Image Correlation

FEM Finite Element Method

Acknowledgment

I would like to thank my supervisor, Professor Luca Goglio, for allowing me to pursue the first stage in developing an academic career. This opportunity opened the gate to a better understanding of physical phenomena and broadened my skills and knowledge in the field that directly affects modern engineering. His insight and guidance throughout this journey have been invaluable to my personal development.

Besides my supervisor, I genuinely acknowledge the kind assistance of Ing. Raffaele Ciardiello, Ph.D. students Boursier Carlo Niutta and Fiumarella Dario, who guided me and supported me throughout this work. Their feedback, ideas, and knowledge have been very beneficial for me.

I want to thank my family and friends, specifically from the Politecnico di Torino, for providing me extra confidence throughout my master's degree. At last, I dedicate my thesis to my late father; without his tireless efforts, I could not be here where I am now.

Abstract

Due to the outstanding advantages, adhesive joining technology is widely used in engineering applications, particularly in the automotive industry. Adhesive joints are adopted in many applications involved in crash and impact events; a universally adopted procedure to test the adhesive joints in dynamic conditions has not been standardized or validated. This work aims to develop a model and a methodology that can assess the behavior of the adhesive joints under impact loading and validate it through experimental tests. The parametric study will be carried out on composite and steel substrates bonded with an adhesive used in the automotive industry using LS-Dyna for the numerical simulations.

Chapter 1 : Introduction

1.1 Motivation

To minimize fuel consumption, automotive and aerospace manufacturers are trying every possible solution to reduce the weight of the structures. Structural adhesive joints are one of the possible solutions for them; this engineering solution helps them join two or more parts together without modifying the parts' parent mechanical properties. Industries use the structural adhesive to join similar or dissimilar metal, polymers, and composite materials; unlike the traditional joining process welding or mechanical fasteners, the bond does not have any problem with galvanic corrosion. Moreover, the use of adhesive potentially increases the energy absorption ability of the structure.

As with the advent of technology, numerical simulations were developed, which are economical and reasonably practical. But as usual, the numerical results are always good, but only numerical results cannot give us the complete picture of the phenomenon in the actual experiment. In the numerical simulations, many mechanical properties are needed, which cannot be achieved without performing the experiment results.

Although it is a very complicated and challenging task to develop the constitutive model, the researcher developed some models to simulate these adhesive-bonded models. One of them is an implication of the tiebreak nodes, which is the simplest one that requires the failure strength in tensile and shear; it can be suitable for the quasi-static test but not so good for the dynamic test. The second one is the cohesive elements which are a bit complex than tiebreak nodes but has good accuracy. The cohesive elements that require peak traction in normal and shear direction and the energy release rate and strain rate effects can also be included. The third is the continuum approach which is a more complicated and complex one. Sometimes including the damage mechanics formulations, it can predict the crack imitations and crack growth.

Most of the surveyed literature includes vast information and data regarding the bonded structures' quasi-static test, but for the dynamic testing, it still lags some information. As for

the impact properties of the structural adhesive, there are still some unfolded parameters and properties.

1.2 Objective

The mechanical behavior of the structural adhesive joints in the quasi-static tests is known. They are easy to find, but in the case of dynamic tests, it is still in the developing stages, and several solutions were presented in the literature. However, in the drop dart testing of the adhesive bonded joints is not explored enough. Adhesive Butt joints are generally used to evaluate the peeling behaviors of the structural adhesive in the quasi-static test, i.e., tensile test. This work aims to analyze the parametric study of the Adhesive butt joint in the drop dart test, obtaining the specific geometry using the numerical simulation, which gives only the shear behavior under the drop dart loading conditions on metallic and composite materials—and validating these numerical simulations with the experimental results.

Chapter 2 : Literature Review

2.1 Joining Process

For every manufactured product after the machining processes, there are some essential welding and joining methods.[1]. However, all these joining processes are different from each other regarding their techniques, properties, and cost. The parts where they are joined with each other are called joints. In the assembly, the joint transmits and distributes the force during the service, i.e., loading. [2]. Riveting is considered the most ancient joining process before riveting holes have to be drilled in the part that reduces the parts' strength. While joining, it also creates a galvanic difference that leads to galvanic corrosion. With the evolution of technology, more joining processes are discovered like welding, soldering, and adhesive bonding. Every joining process has cons and pros, like some are permanent, and others are temporary. The joining processes are mainly categorized into three main types in fig 2.1; further classification of these joining processes is shown.

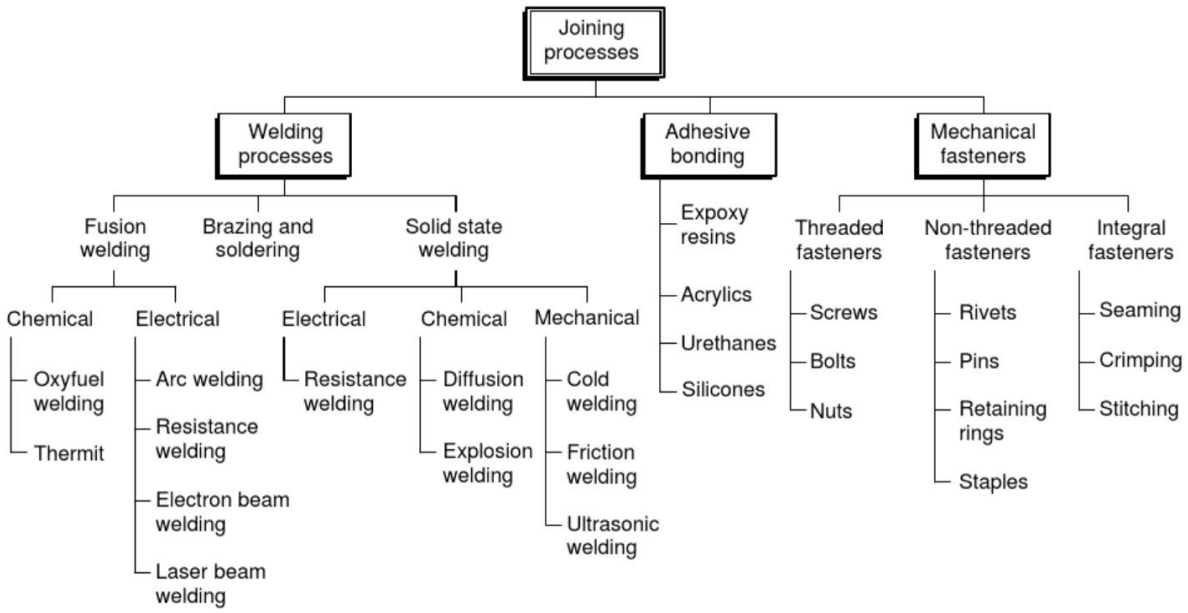

Figure 2.1 *General Classification of the joining processes* [3]

Generally, there are five most used types of joints: butt, tee, lap, corner, and edge joints. In fig 2.2 type of joints is shown. The choice of joining process and the kind of joint to be used is based on several considerations: cost of production, manufacturability, reliability,

aesthetics, repairability, etc. But the choice of joining process also depends on the material type, thickness, geometry, and joint location.

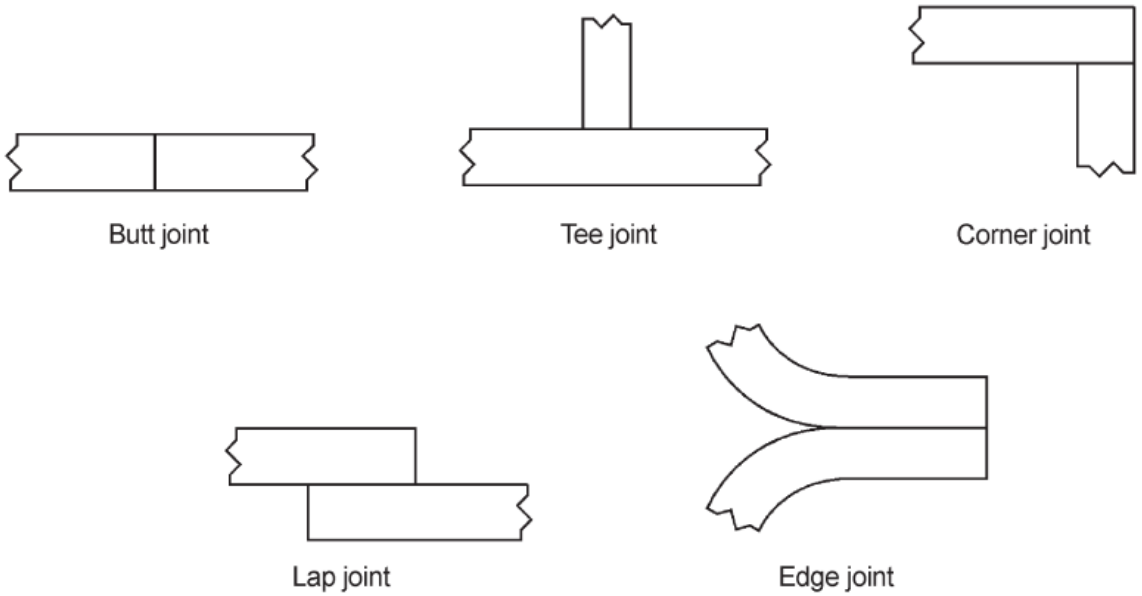

Figure 2.2 *Types of Joints* [4]

2.2 Adhesive Bonding

In ancient times' animals and the plant were the only source of the adhesives. Still, with the evolution of scientific knowledge, various polymerization processes were developed, which creates plenty of bonds. The adhesive bonding joining process is widely used in the automotive and aerospace industries lately at the end of the 20th century. The pieces or the parts that are joined by the adhesive are called adherends or substrates. Adherends can neither be similar or dissimilar metals, composites, glass, plastic, or other substrate material. In history, the adhesive forms a weak bond but now adhesive creates a strong bond and distributes the load stress evenly on the bonded structure, making the joint strong. Sometimes it also provides an aesthetic look as an adhesive is invisible in the assembly. [2]. They are better than other types of joining because it avoids the corrosion defect which is the main problem while joining two dissimilar metals. The weight reduction characteristics of the adhesive material give plenty of benefits to the automotive and aerospace industry; as a result, a lot of research is conducted in this emerging field of engineering. The adhesive bonding provides better stiffness characteristics than other mechanical fastenings because it provides stiffness to all the bonded areas.

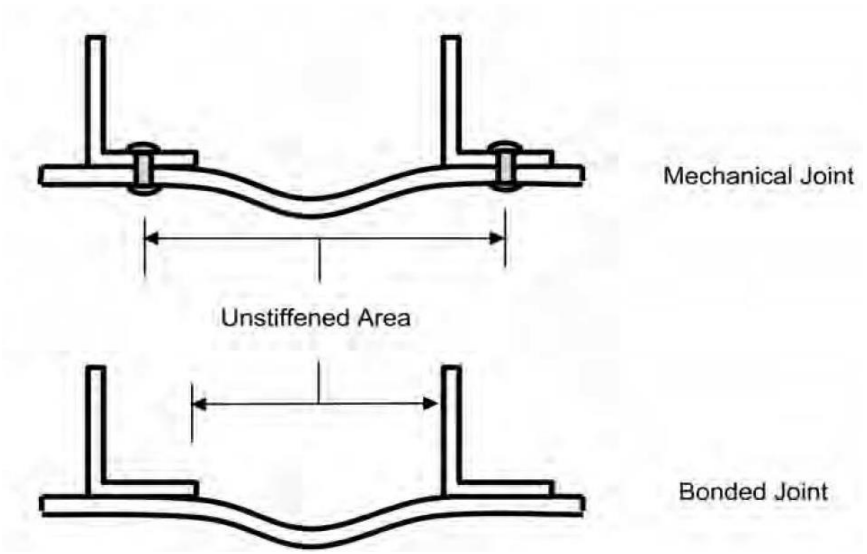

Figure 2.3 *Load distribution comparison for mechanically fastened and bonded joints* [5]

Adhesive bonding can be categorized into two principal types: structural and nonstructural adhesive. [6]. Structural adhesives are used when the bonded structure is subjected to more stress but under the yield point. On the other hand, nonstructural adhesives are weak adhesive and cannot withhold a higher load; they can keep the light material when joined. Adhesive bonding can also be categorized based on the chemical structure or functionality, such as natural and synthetic.[6]. The natural group came from organic sources such as vegetable starch, animal glue, or some protein-based adhesives. On the other side, synthetic adhesives are based on elastomers, emulsions, thermosets, and thermoplastics. Several adhesive materials are available in the market, but their usage depends on the applications, type of adherends, and the bonding process.

2.2.1 Thermosetting Adhesives

These are the material after initial curing; these cannot be softened while heating. Once these are cured and cross-linked, these can be softened upon heating, but it is impossible to achieve their initial state. This adhesive can be cured at room temperature or elevated temperature. When heated at a relatively high temperature than their curing temperature, such an adhesive usually degrade and weakened due to the oxidation or molecular chain session.[7]. Thermosetting adhesives are densely crosslinked; under loading at elevated temperatures, they show slight deformation. [8]. In this work, two types of thermosetting adhesive are used, which are epoxy and polyurethane.

2.2.2 Thermoplastic Adhesives

These types of adhesives are different from that of thermosetting because they become soft or melt upon heating. They can be melted or soften upon heating; means we can achieve them in their initial state. This type of adhesives can also be dissolved in a solvent to produce a flowable solution and then rehardened to evaporate the solvent. [7]. Thermoplastic adhesives have a more limited operating temperature range than thermosetting types. Although certain thermoplastics may provide excellent tensile shear strength at relatively moderate temperatures, these materials are not crosslinked and will tend to creep under load at lower temperatures.

2.3 Adhesive Joints Failure Modes

A couple of theories explain the adhesion processes related to the microscopic, macroscopic, molecular, and atomic scale of actions. Few of these theories are famous, like mechanical interlocking, diffusion, wettability, and weak boundary layer.

If there is a failure in the adhesive layer rather than the adherends, it is called adhesive failure. In adhesively bonded structures generally, there are three types of failure; one is called the cohesive failure in the adhesive layer. The second failure may occur due to the poor bonding of the adhesive and adherend interface, or the adhesive is so strong that it does not fail. Still, the interface between the adherend and the bond separates. The third one is the bond is so strong that the adherend fails, but the adhesive did not, as shown in **figure 2.4**.

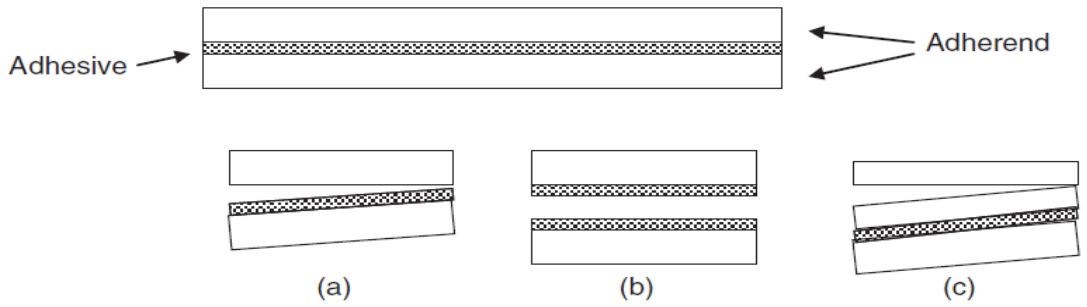

Figure 2.4 *Adhesive failure modes schematics: (a) adhesive failure, (b) cohesive failure in the adhesive layer, and (c) failure in the adherend* [9]

Adhesive joints can either fail in adhesive mode or in cohesive mode. Cohesive failure is usually appreciated rather than adhesive failure because the maximum strength of a material in a joint is reached. But if there is an adhesive failure, this may indicate a surface preparation problem responsible for decreased joint durability.

The composite bonded joint failure is different from that of the one that we see in the metals, but the prediction of composite bonded joint failure is difficult. According to the ASTM standard D5573 – 99, there is a classification of failure modes in the composite material.

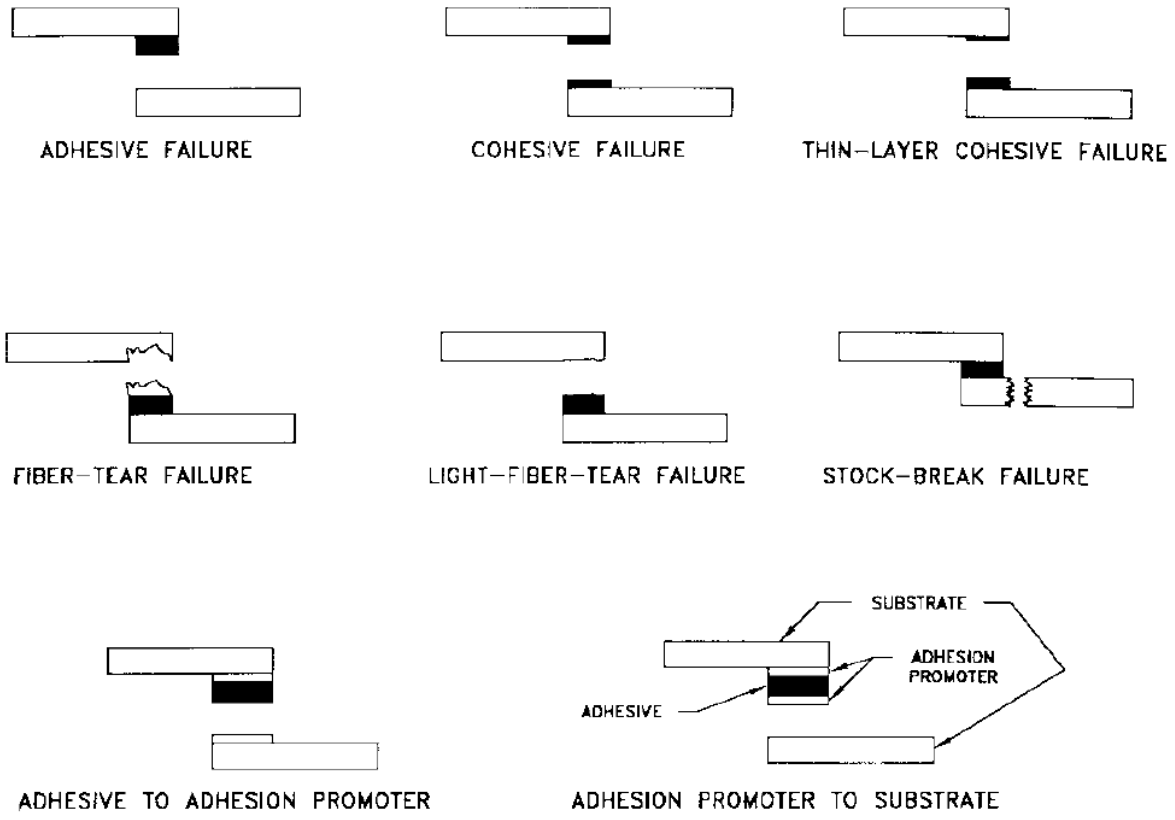

Figure 2.5 *Schematic representation of the failure modes in the composite material* [10]

2.4 Adhesive Mechanical Properties Characterization

There are several stress states experienced for an adhesive joint while submitted to typical loading conditions. Specialized test coupons are designed for material characterization to measure specific properties. The measured properties of an adhesive are dependent on the mode of loading; Mode I is the tension, Mode II is in-plane shear and Mode III out-of-pane

shear, but this one is not very common. The properties of an adhesive required for material models often include Young's modulus, the tensile and shear strengths, and the fracture toughness (more specifically, the energy release rate) in Mode I and Mode II.

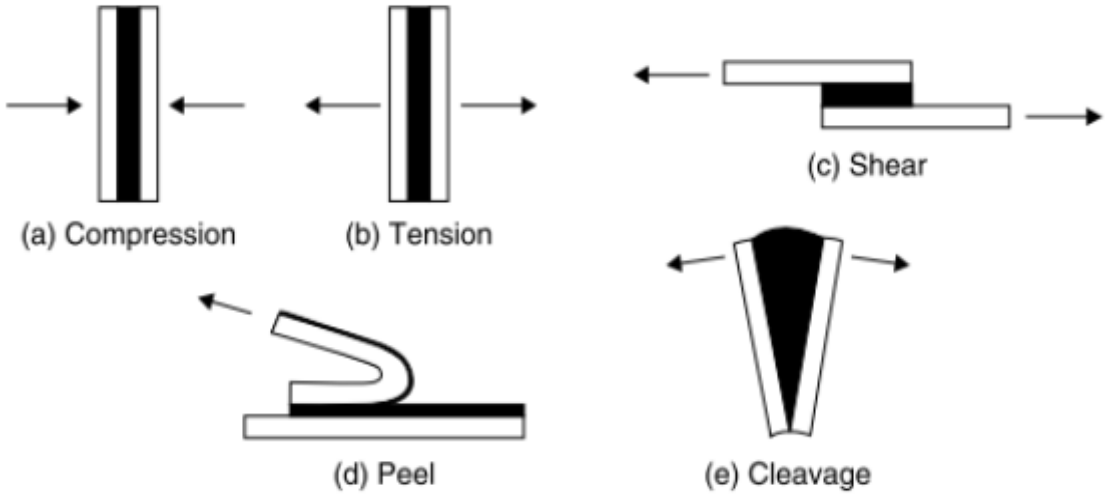

Figure 2.6 *Stress states of adhesive joints [11]*

Traditionally for the Mode I critical energy release rate (G_{IC}) of an adhesive is achieved by the standardized mechanical tests; usually, that test is the Double Cantilever Beam (DCB) or Tapered Double Cantilever Beam (TDCB) by using ISO 25217-2009 [12] and also by using ASTM. [13]. In both tests, two beams are bonded with the help of adhesives and loaded in tension until crack propagates in the joint, and from this, the critical energy release rate is calculated.

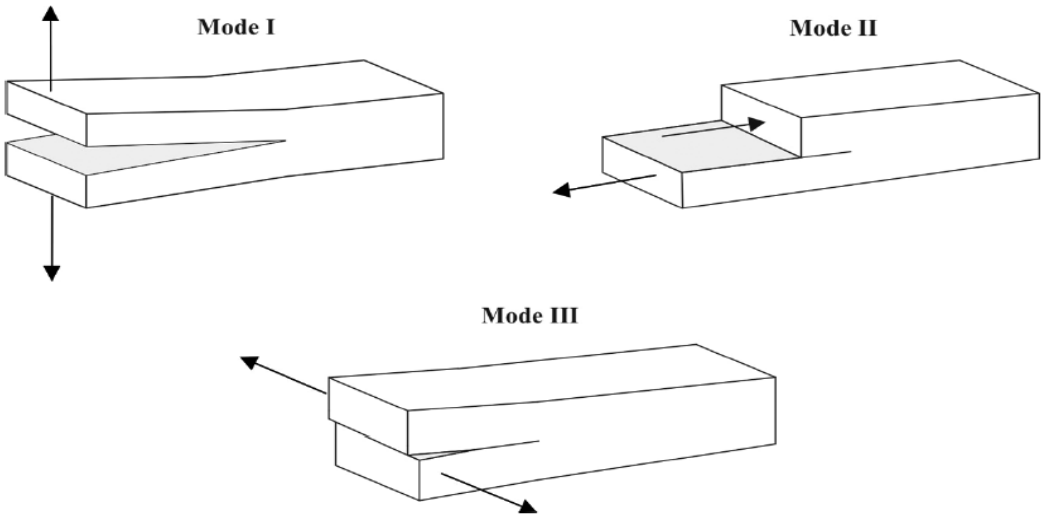

Figure 2.7 *Adhesive joint fracture modes [14]*

But this parameter is not enough to describe the traction separation response in the Mode I, to define it fully the peak value and the initial stiffness is required, which are calculated by performing further test which is usually butt-joint testing. Additionally, for describing the adhesive behavior more precisely, strain rate dependency has to be checked for high-rate testing. As the standardized specimens of DCB and DTCB have a high mass and introduce inertial effects when loaded to higher velocity, this is a challenge. [15].

The solution of this problem was proposed by Dasterdi et al. that to use the rigid double cantilever beam (RDCB) geometry to measure Mode I traction separation response using a single test. [16]. The analysis done by Dasterdi et al. assumed that the rigid adherends rotate at the other end, which is far from the loading pins.

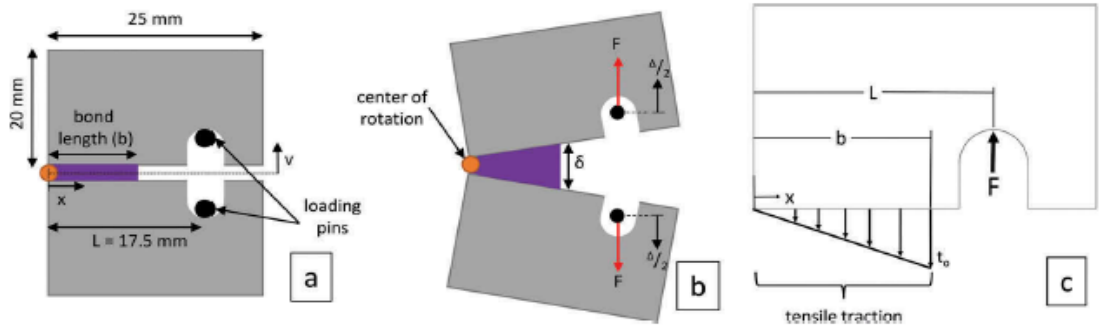

Figure 2.8 *(a) Dimensions used in the Analysis, (b) loading schematic, (c) free body diagram [15]*

Later it was discovered that some part of the joint was in the compression, and analysis was modified in such a way that the center of rotation was displaced to an arbitrary distance μ from the end away from the loading pins, to obtain Mode I traction separation response of adhesive. [15].

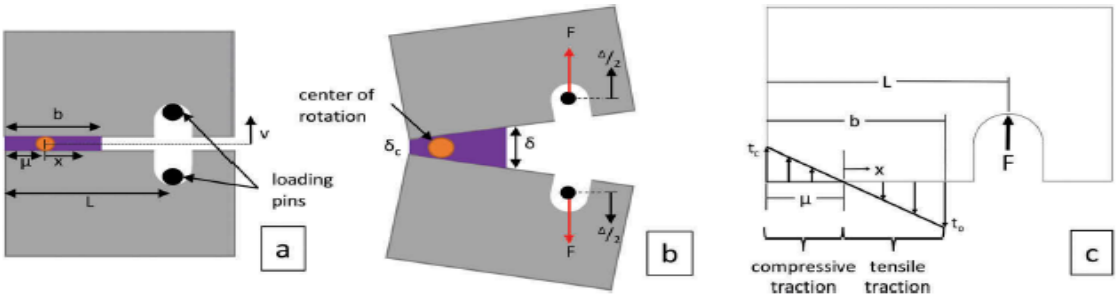

Figure 2.9 *(a) dimension used in the analysis, (b) loading schematic, and (c) updated free body diagram. [15]*

For the Mode II the critical energy release rate (G_{IIC}) is usually obtained by performing end-loaded split (ELS), end notch flexural (ENF), or four-point end notched flexural (4NF) tests. [17]. The ENF is the most used test to obtain the Mode II fracture properties. However, if the specimen dimensions were not selected accurately, there is still a problem of unstable crack growth. Additionally, as in the case of Mode I characterization, the shear strength of adhesive can also be obtained by performing additional tests. The most common of them is sing lap shear or thick adherend lap shear test. Single lap shear is a pretty simple one. Still, there is a problem while loading there is a rotation of joint, as a result, which introduced the peel stresses in the adhesives that can affect accuracy shear strength characterization. [18].

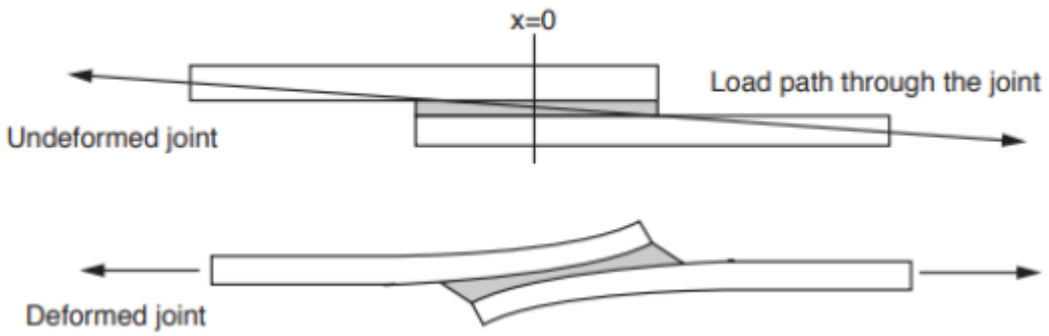

Figure 2.10 *Undeformed and deformed single lap joint. [18]*

Making the adherends thick reduces the bending of the adherends and reduces the mixed-mode loading; as a result, better shear properties can be obtained.

2.5 Numerical Modelling of Adhesive Joints

The Finite Element Method (FEM) is the most used numerical method for structural and thermal problems. In FEM, the domain is discretized into several small elements. The material is also modeled with the series of elements for the adhesive-bonded joint problem for the adherends and adhesive itself. Hrennikoff first founded this technique in 1994. [19]. As the technology is progressing and with the rapid computing power, the FEM technique is widely used in automotive and aerospace applications and becoming the essential tool for

many engineering problems. The adhesive material can be modeled in three ways one way is defining them by tiebreak contact between the adherends, second is representing the adhesive by cohesive elements, and last is representing it by continuum solid elements.

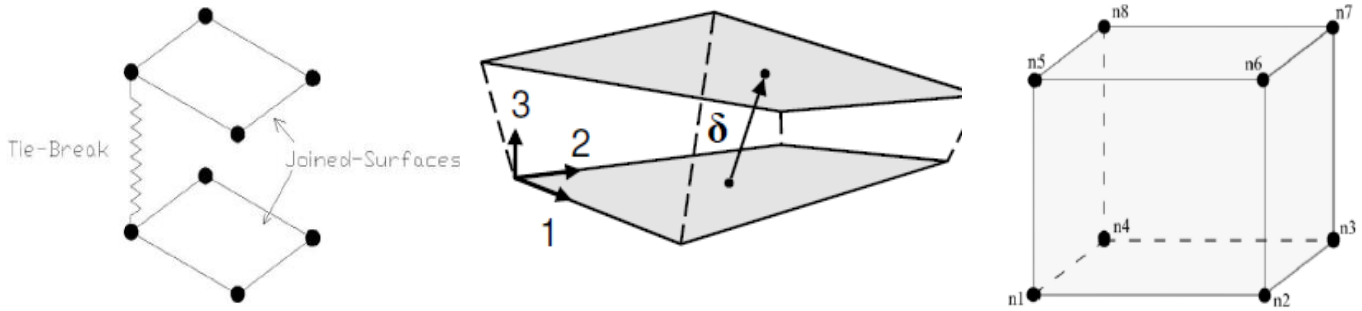

Figure 2.11 *Adhesive joint representation by numerical methods (a) tie-break contact, (b) cohesive elements, and (c) solid continuum elements [20]*

In tie-break contact, a spring connection is defined between two nodes, and each of these nodes belongs to the different bodies. It is a straightforward model to simulate the adhesive joint because failure normal or shear stress or both are required.

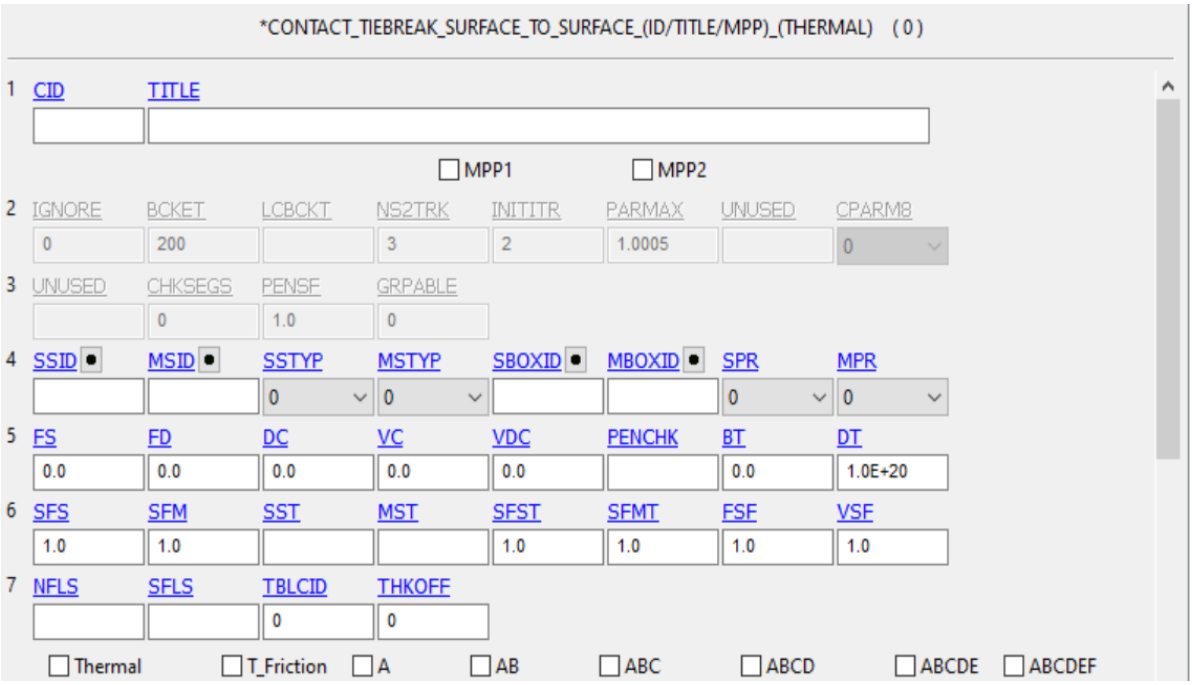

Figure 2.11 *Properties required to define tie-break contact between two surfaces.*

Where.

SSTYP: Slave segment set or node set type.

MSTYP: Master segment type.

NFLS: Tensile failure stress.

SFLS: Shear failure stress.

Damage is initiated when the stress reaches a failure criterion. Due to its simplicity, very few computational resources are required, but it is sometimes tricky to thoroughly observe the adhesive joint response. As the crack propagates, the first contact between the nodes fails, and suddenly it passes to the next set of nodes. This phenomenon continues from one element to another one which is known as numerical unzipping.

The second numerical method to represent the adhesive is the cohesive elements, which overcome the limitations of the tie-break contact. In this method, the joint is described as one spring between nodes but a series of springs between the two joining surfaces. Thus, there are three springs, one in normal and two in shear. Unlikely tie-break contact, these are defined by the elements, and then the material model is assigned to these elements.

This approach is quite efficient in terms of computation and capable of predicting the material's response in the Mode I and the Mode II. Therefore, the technique is widely used for numerical modeling of the adhesive joints, and some of the material models can also be capable of deal with the strain rate effects.

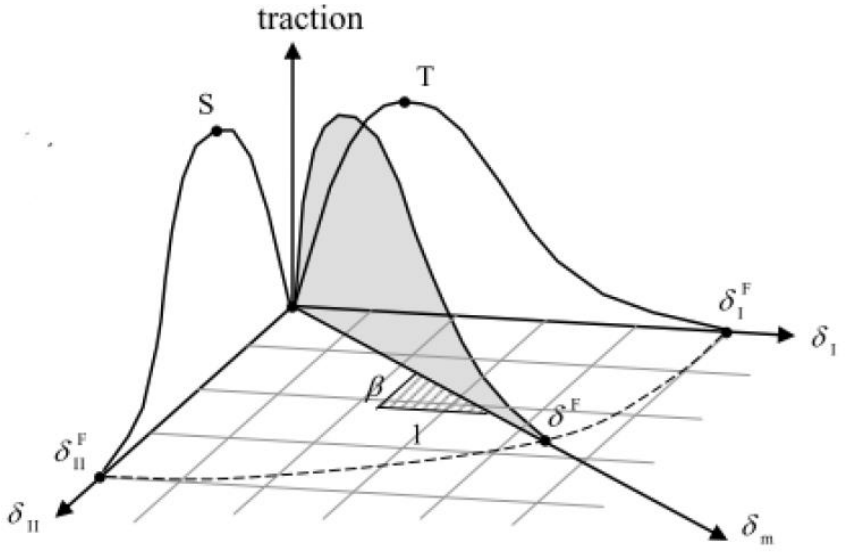

Figure 2.12 *Traction-Separation law includes the mixed-mode response.*

The third approach to simulate a numerical representation of adhesive joint is by continuum elements is very sophisticated. It describes the linear elastic-plastic behavior, viscoelasticity, and viscoelastic plastic behavior. It requires more computational power and time, but it incorporates damage mechanics or cracking formulation and propagation. [21] This approach gives a more physical formulation of the adhesive joint.

In this work cohesive element approach is used for the modeling of the adhesive material.

2.5.1 Mat 138 (Mat Cohesive Mixed Mode)

Mat 138 is a way to model the adhesive material cohesively; it is a simplified model that features a triangular traction separation law. Regardless of its simplicity, if it is properly calibrated, then it guarantees invaluable results with the structural adhesives that this work enlightens. It includes a bilinear traction-separation law with quadratic mixed-mode delamination criterion and a damage formulation. It should be used only with cohesive element formulations.

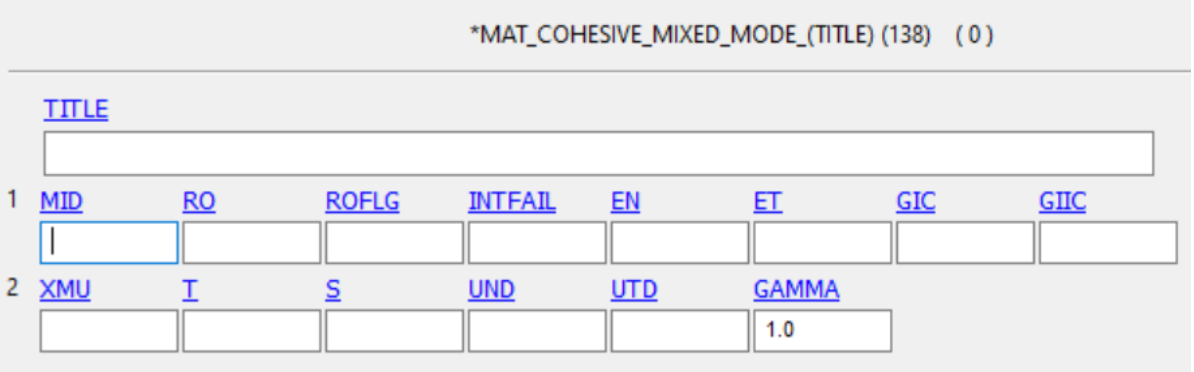

Figure 2.13 *Properties required for Mat 138 Cohesive Mixed Model.*

Where.

RO: Mass density.

EN: The stiffness normal to the plane of the cohesive element.

ET: The stiffness in the plane of the cohesive element.

GIC: Energy release rate for mode I.

GIIC: Energy release rate for mode II.

T: Peak traction in a normal direction.

S: Peak traction in a tangential direction.

UND: Ultimate displacement in the normal direction.

UTD: Ultimate displacement in the tangential direction.

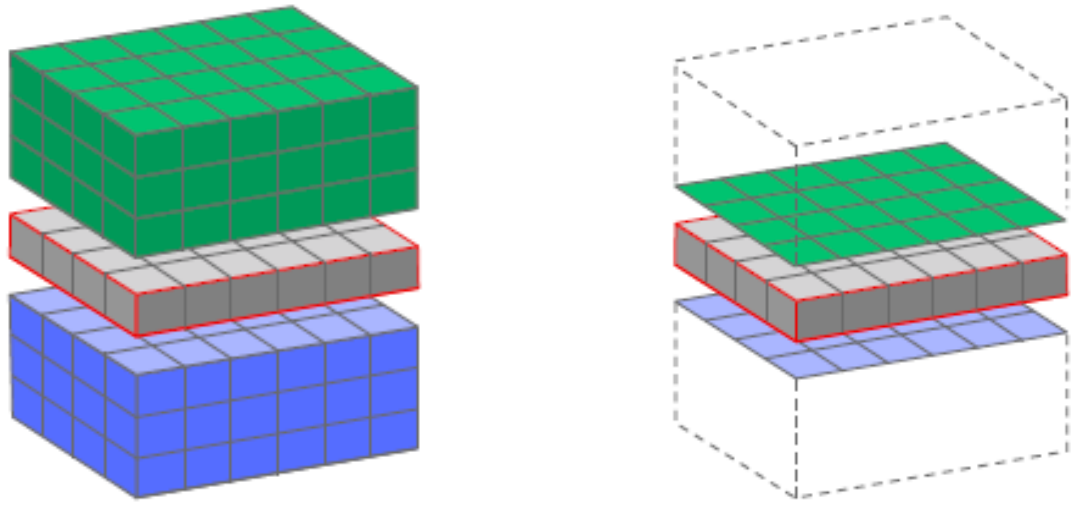

(a) (b)

Figure 2.14 *(a) 8 - node type 19 elements, (b) 8 – node type 20 elements*

It is a purely elastic cohesive zone model with damage and does not have plasticity. The ultimate displacements in the normal and tangential directions are the displacements when the material has failed, i.e., the tractions are zero. [20]. The linear stiffness for loading followed by the linear softening during the damage provides a straightforward relationship between the energy release rates, the peak tractions, and the ultimate displacements:

$$G_{IC} = T \times \frac{UND}{2}$$

$$G_{IIC} = S \times \frac{UTD}{2}$$

If the peak tractions are not specified, they are calculated from the ultimate displacements. In this model, the total mixed-mode relative displacement δ_m is defined as

$$\delta_m = \sqrt{\delta_I^2 + \delta_{II}^2}$$

where $\delta_I = \delta_3$ is the separation in the normal direction (mode I) and

$$\delta_{II} = \sqrt{\delta_1^2 + \delta_2^2}$$

δ_{II} is the separation in the tangential direction (mode II). The mixed-mode damage initiation displacement δ^0 (onset of softening) is given by

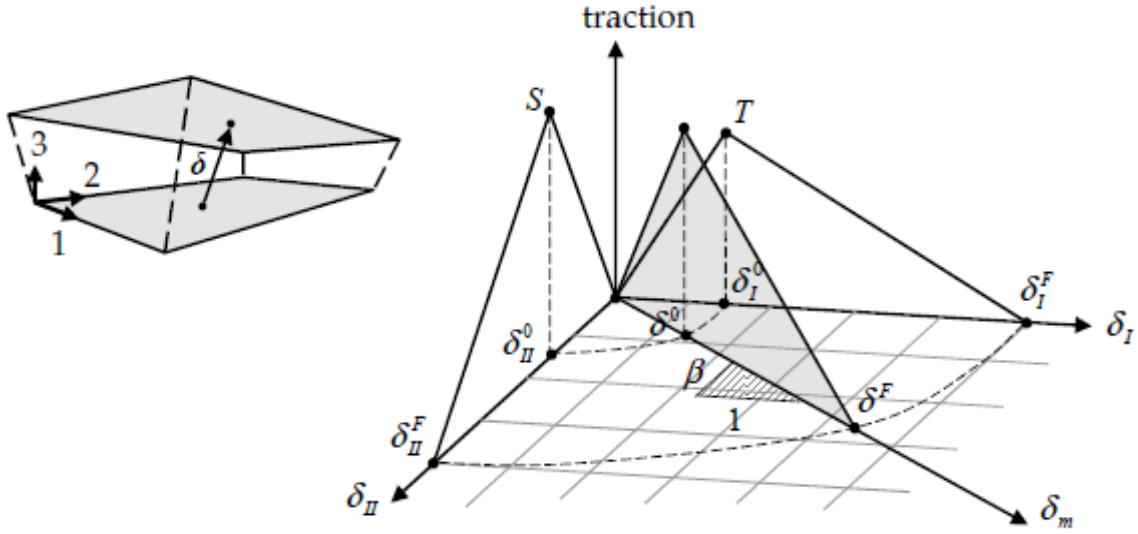

Figure 2.15 *Mixed-mode traction-separation law [20]*

$$\delta^0 = \delta_I^0 \, \delta_{II}^0 \sqrt{\frac{1+\beta^2}{(\delta_{II}^0)^2 + (\beta\delta_I^0)^2}}$$

Where $\delta_I^0 = {}^{T}/_{EN}$ and $\delta_{II}^0 = {}^{S}/_{ET}$ are the single-mode damage initiation separations and $B = {}^{\delta_{II}}/_{\delta_I}$ is the "mode mixity." The ultimate mixed-mode displacement δ^F (total failure) for the power law (**XMU** > 0) is: Formulation 1

$$\delta^F = \frac{2(1+\beta^2)}{\delta^0}\left[\left(\frac{EN}{GIC}\right)^{XMU} + \left(\frac{ET}{GIIC}\right)^{XMU}\right]^{\frac{1}{XMU}}$$

$$\left(\frac{GI}{GIC}\right)^{\alpha} + \left(\frac{GII}{GIIC}\right)^{\alpha} = 1$$

Formulation 2: Benzeggagh – Kenane (**XMU** < 0) :

$$\delta^F = \frac{2}{\delta^0 \left(\frac{1}{1+\beta^2}\mathrm{EN}^\gamma + \frac{\beta^2}{1+\beta^2}\mathrm{ET}^\gamma\right)^{1/\gamma}} \left[\mathrm{GIC} + (\mathrm{GIIC} - \mathrm{GIC}) \left(\frac{\beta^2 \times \mathrm{ET}}{\mathrm{EN} + \beta^2 \times \mathrm{ET}}\right)^{|\mathrm{XMU}|}\right]$$

$$GC = GIC + (GIIC - GIC) \left(\frac{GII}{GI + GII}\right)^{\eta}$$

A suitable choice for the exponent γ would be GAMMA = 1.0 (default) or GAMMA = 2.0.

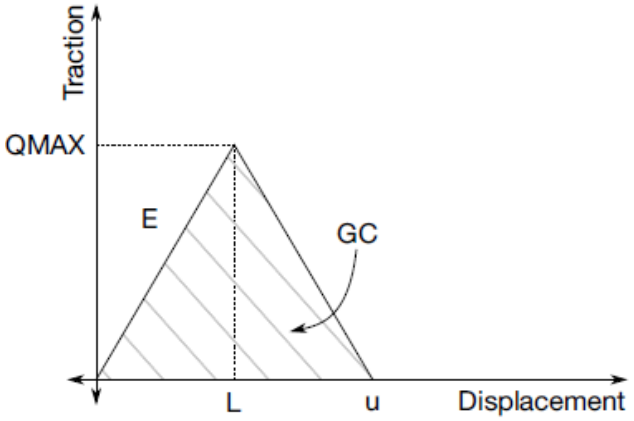

Figure 2.16 *Bilinear traction-separation*

Two errors checks must be put into effect for this material model to ensure accurate material data. Since the traction versus displacement curve is simple (triangular shaped), equations can be established to provide that the displacement, L, at the peak load (QMAX), is smaller than the ultimate distance for failure, u. [20].

First one is

$$\mathrm{GC} = \frac{1}{2}\, u \times QMAX$$

And the second is

$$L = \frac{QMAX}{E}$$

To make sure that the peak is not over the failure point, $\frac{u}{L}$ Must be greater than 1.

$$u = \frac{2GC}{EL}$$

The above two equations give

$$\frac{u}{L} = \frac{2GC}{EL \times L} = \frac{2GC}{E\left(\frac{QMAX}{E}\right)^2} > 1.$$

This error check is done for both cases, i.e., for tension and shear, respectively.

2.5.2 Mat 240

(Mat Cohesive Mixed Mode Elastoplastic Rate)

This model looks similar to Mat 185, but it includes strain rate dependency and plasticity. In addition, it comprises a tri-linear traction-separation law with a quadratic yield and damage initiation criterion in mixed-mode loading (mode I - mode II). In contrast, in this model, the damage evolution is controlled by a power-law formulation. Therefore, the model is suitable only for cohesive element formulations (Elform 19-20).

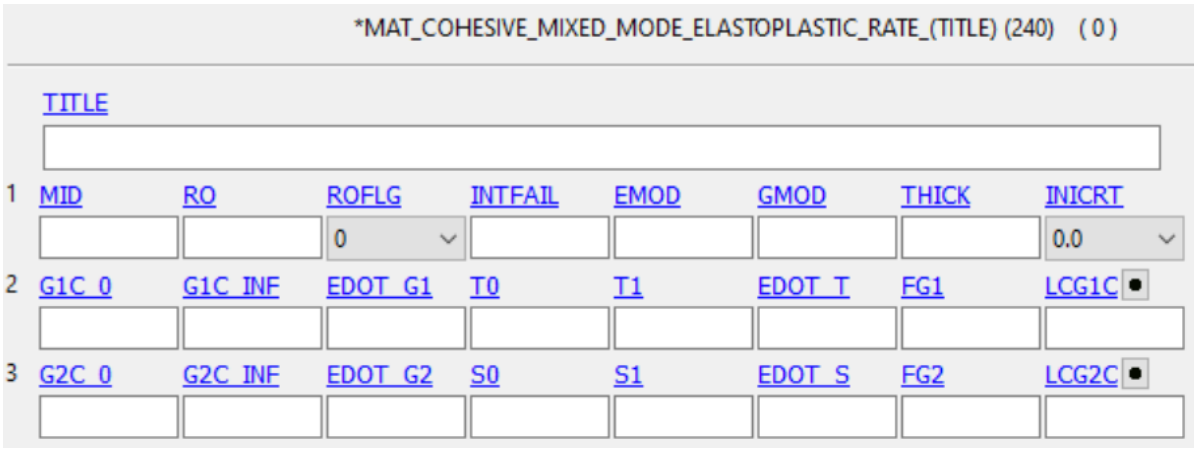

Figure 2.17 *Parameter required for Mat 240*

RO = Mass density

ROFLG = Flag for whether density is specified per unit area or volume. ROFLG = 0 specified density per unit volume (default), and ROFLG = 1 determines the density is per unit area for controlling the mass of cohesive elements with an initial volume of zero.

EMOD = Young's modulus of a material (Mode I).

GMOD = Shear modulus of a material (Mode II).

G1C_0 = Energy release rate G_{IC} in Mode I.

G1C_INF = Upper limit value of the rate-dependent G_{IC} (only considered if Energy release rate G_{IC} in Mode I is less than zero. i.e., G1C_0 < 0).

EDOT_G1 = Equivalent strain rate at the yield initiation to define the rate dependency of G_{IC} (only considered if G1C_0 < 0)

T0 = Yield stress in Mode I.

T1 = It is only considered, when T0 < 0, [GT.0.0: Quadratic logarithmic model and LT.0.0: Linear logarithmic model]

EDOT_T = Equivalent strain rate at yield initiation to describe the rate dependency of the yield stress in Mode I (only considered if T0 < 0)

FG1 = It is used to elaborate the tri-linear shape of the traction-separation law in Mode I

G2C_0, G2C_INF, EDOT_G2, S0, S1, FG1, and **EDOT_S** are the parameters that are defined in Mode II.

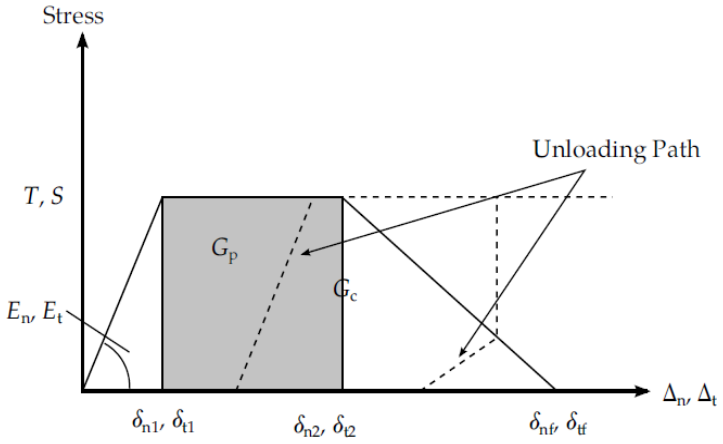

Figure 2.18 *Trilinear traction separation law [20]*

The separations Δ_n in mode I, which is a normal one (peel) and Δ_t in mode II, which is tangential (shear), directions are determined from the element's separations in the integration points,

$$\Delta_n = \max\ (\ u_n\ , 0\ )$$

And

$$\Delta_t = \sqrt{u_{t1}^2 + u_{t2}^2}$$

Where u_n , u_{t1} and u_{t2} are the separations in normal and in both tangential directions of the element coordinate system. The total mixed-mode separation (Δ_m) is determined by

$$\Delta_m = \sqrt{\Delta_n^2 + \Delta_t^2}$$

The initial stiffnesses in both modes are calculated from the elastic Young's and shear modulus and are respectively,

$$E_n = \frac{EMOD}{THICK}$$

$$E_n = \frac{EMOD}{THICK}$$

Where THICK is an input parameter which is the element's thickness. Unless the input THICK > 0 is computed from a distance between the element's corner nodes (Nodes 1-5, 2-6, 3-7, and 4-8, respectively).

for mode I loading:

$$0 \le f_{G1} = \frac{G_{I,p}}{G_{IC}} < 1 - \frac{T^2}{2G_{IC}E_n} < 1$$

for mode II loading:

$$0 \le f_{G2} = \frac{G_{II,p}}{G_{IIC}} < 1 - \frac{S^2}{2G_{IIC}E_t} < 1$$

As a recommended alternative, the shape of the tri-linear model can be described by the following displacement ratios (triggered by negative input values for f_G):

for mode I loading:

$$0 < |f_{G1}| = \left|\frac{\delta_{n2} - \delta_{n1}}{\delta_{nf} - \delta_{n1}}\right| < 1$$

for mode II loading:

$$0 < |f_{G2}| = \left|\frac{\delta_{t2} - \delta_{t1}}{\delta_{tf} - \delta_{t1}}\right| < 1$$

While f_{G1} and f_{G2} are always constant values, T, S, G_{Ic} and G_{IIc} may be selected as functions of an equivalent strain rate $\dot{\varepsilon}_{eq}$, which is evaluated by

$$\dot{\varepsilon}_{eq} = \frac{\sqrt{\dot{u}_n^2 + \dot{u}_{t1}^2 + \dot{u}_{t2}^2}}{THICK}$$

where $\dot{u}_n$, $\dot{u}_{t1}$ and $\dot{u}_{t2}$ are the velocities corresponding to the separations u_n, u_{t1} and u_{t2}.

2.6 Testing of Adhesively Joint

Adhesive structural bonds are strong bond which can sustain load at different loading rates and different loading conditions. As a result of the viscoelastic behavior of adhesives, they are pretty sensitive to the loading rate.[22]. The testing of adhesives is required to characterize the adhesives joint design. The study of the dynamic behavior of the structural adhesive joints became very popular in the last two decades. [23]. Generally, two issues arise about the behavior of an adhesive subjected to impact. The first one is whether an abrupt loading can cause brittle behavior in a material that under static or quasi-static conditions would not be brittle; this aspect is critical regarding the capability of absorbing energy. The second issue is assessing the influence of the loading rate on the adhesive response, i.e., the sensitivity of the adhesive properties to the strain rate. [24]. Various impact tests have been devised using many methods to apply the sudden loading and use multiple parameters to characterize the impact performance. [25]. In reality, the impact test is differentiated into three ranges: lower velocity, up to 5 m/s, medium velocity from 5 to 10 m/s, and high velocity from 10 to 100 m/s. [26]. One standard test, the ASTM Block Impact Test D950 and ISO 9653 are used to determine the impact strength of adhesive bonds, mainly in the shear employing a test rig similar to that used for Izod resilience measurement. [24].

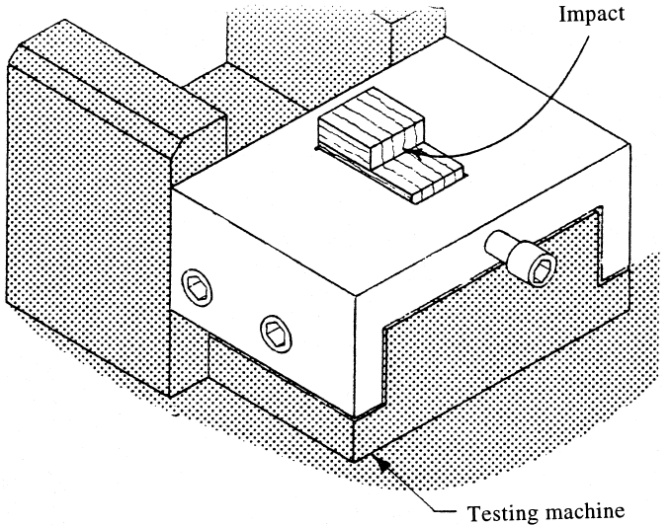

Figure 2.14 *The ASTM D950-82 Impact Test.* [22]

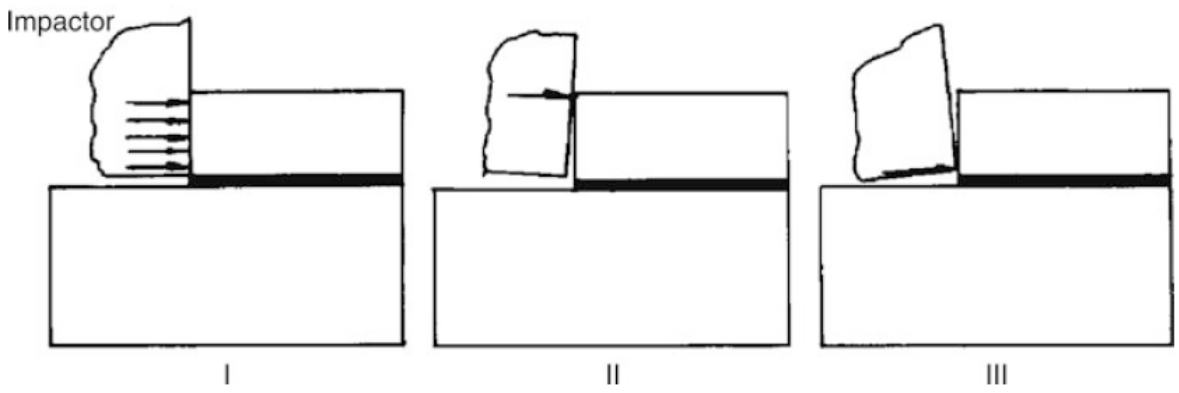

Figure 2.15 *Three possibilities of loading case for ASTM Block Impact Test Specimen [25]*

The case (I) seems to be an ideal without any misalignment, but the stresses present in the adhesive are the shear stress peaks near the bond end at the impacted side. Also, the peel stress is significant and peaks near the bond end at the impacted side; then, it decreases monotonically, assuming a negative sign at the opposite bond end. In case of misalignment, shear and peel stress distribution is strongly affected because of the changing of moment value and local compressive deformation of the block. [25]. Another solution is provided that using a specimen consists of rod bonded into a cylinder segment. [22].

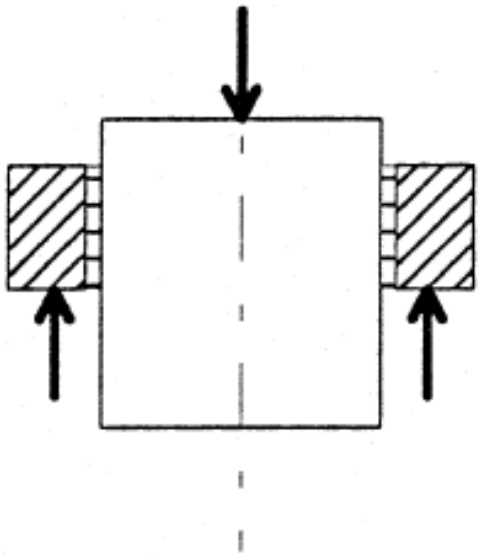

Figure 2.16 *Specimen design of cylindrical segment [22]*

The stain and stress obtained are not shear as expected, but there is a presence of the normal stresses, but there is lesser sensitivity of the misalignment than the specimen suggested by the standard ASTM D950-82.

Another standard is called the "Impact wedge peel test" by ISO 11343:2003, EN ISO 11343:2005, and EN ISO 11343:2019. The two metallic strips are formed of the specified dimensions and are bonded together to obtain the geometry shown below.

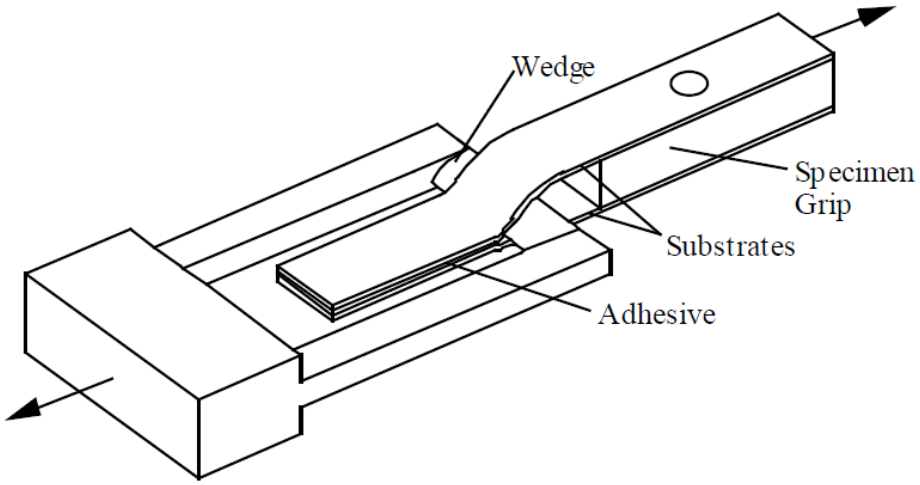

Figure 2.17 *Impact wedge peel test specimen [27]*

The specimen is loaded by a wedge with one side of a rectangular shackle and goes through the bond, thus separating the metallic strips in peeling mode. There is a typical 2 m/s test speed in this test, but the deviation from this test speed is possible, and the maximum bond thickness shall be 2 mm. [28]. Two types of crack growth were observed stable and unstable. In case first case, i.e., stable crack growth, the crack tip runs ahead of the wedge at the constant offset, but in the second case, i.e., in the unstable crack growth, the crack propagates rapidly through the whole adhesive bond than that of the wedge. If the crack growth was stable, then the results are acceptable, but it may lead to false results in the case of unstable. [27]. And in the standard EN ISO 11343:2019, if the tested material provides the highly irregular force curves, then the test results must be discarded. [28].

The previous two tests mentioned above have the restriction that the strain rate attained in the adhesive cannot be much high, since it usually does not exceed $10^2\ s^{-1}$. [24]. But for

the higher strain rate, another equipment is used, which is called Hopkinson bar technique and, in particular, the Split Hopkinson Pressure Bar (SHPB) is the main testing means to investigate the dynamic behavior of the materials at medium to high strain rate ($0.5 - 5 \times 10^2\ s^{-1}$). [26]. The Split Hopkinson Pressure Bar (SHPB) apparatus used nowadays was introduced by Kolsky.

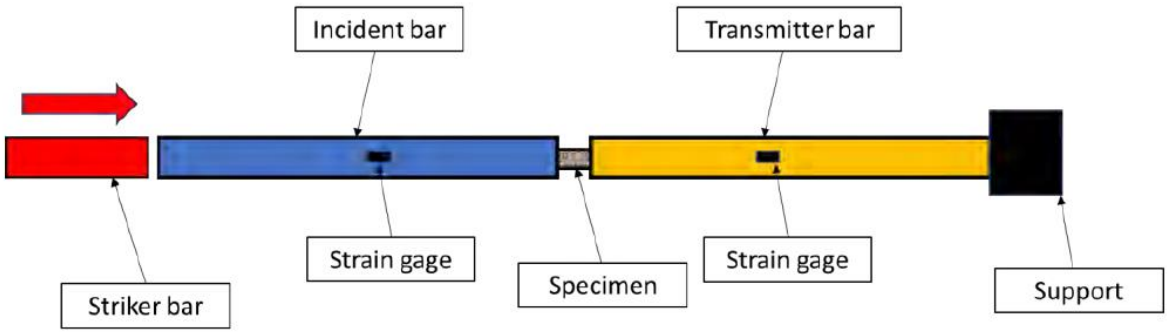

Figure 2.18 *Schematic of a split Hopkinson bar [29]*

The Split Hopkinson Pressure Bar (SHPB) original design is for a compression test, but this test setup is adopted for tension, axial/shear, torsion, and triaxial combination. Due to the different clamping methods other than the original one can be set-ups for the test as mentioned earlier. Yokoyama determined the tensile strength and energy absorption of adhesive butt joints at high loading rates using cylindrical specimens with tensile SHPB. [30]. Goglio et al. have studied the impact of strain rate on the tensile and the compressive strength of the epoxy bi-component adhesive using the SHPB. [31]. Again, Yokoyama et al. have studied compressive stress-strain loop at a higher strain rate for two different bulk structural adhesive using tapered striker with the SHPB. [32]. Yokoyama and Nakai using modified SHPB tension performed impact tests on the hat-shaped specimens and examined the effect of loading rate on an epoxy-based adhesive joint; these specimens are the butt joint made up of aluminum alloy and commercially pure titanium. [33]. Neumayer et al. performed impact loading on the butt and the lap shear specimen and studied the adhesive deformation using the high-speed camera and digital image correlation (DIC). [34].

In the adhesive joining field, the drop dart machines have been used first to generate the impact loading conditions. [24]. The standard impact machine is not much capable of testing the modern toughened adhesives. [35]. Beevers and Ellis have formulated an alternative test

method generally based on drop-weight rigs. This rig established for impact testing contained a crosshead located by low friction bushes on parallel uprights. A rod below the crosshead acted as a guide bar and force transmission element for the drop weight of 10 kg, which can be managed to fall from the 1m height. The force was measured by the means of a strain-gauged transducer mounted on the rig's top frame. The single-lap joint specimen was created both from mild steel and aluminum coupons, bonded with toughened epoxy and was clamped in parallel faced jaws that were also packed on one side to eliminate bending stresses before loading. The drop-weight was raised to 815 mm height so that when released, it will hit the striking platform at 4 m/s. The transient impact force was transmitted to the test piece through the guide rod, and the signals were recorded. As related to the static case, an impact velocity of 4 m/s, the steel joints have shown a significant rise in the ultimate load, but only a slight change has been seen in the case of the aluminum joint. So a different strain rate effect was seen for the two materials. [36]. Jordan described the use of a particular drop-weight tester defined as “instrumented guillotine.” Its peculiar feature was to adjust the impact energy from a maximum of 800 J to a value lower than 100 J and compared the results for epoxy- and acrylic-bonded joints with the riveted or spot-welded ones. [37]. Subsequently, in the DCB and the wedge test, the range of crack velocities acquired was small; Sun et al. performed a drop-tower test on the DCB specimen and a wedge test specimen to achieve higher crack velocities. A drop weight having a mass of 40 kg was released from different heights 20, 30, 40, 50,100, 500, and 1000 mm onto a bonded specimen that was placed on top of a wedge, that wedge was 10 mm away from adhesive, higher velocities were obtained due to this setup. A high-speed camera was focused on the wedge tip, and the scale scribed on the side of the specimen allowed positions of the crack tip and wedge relative to the scale to be monitored as a function of time. Except for a single test performed with a drop height of 30 mm, ‘‘stick-slip” behavior was always noticed. Only in that exception, just quasi-static crack growth was detected, even at crack velocities more than 600 mm/s. Depending on the drop height, the determined average crack velocities that were in the range of about 0.5–5 m/s. [38].

Hayashida et al. have studied the impact behavior of high strength pressure sensitive adhesive (PSA). They have performed impact tests on butt joint specimen and double cantilever beam specimen using the drop-weight impact testing machine with a 2 m/s

velocity; the total weight, i.e., the sum of the drop weight and the impactors, was almost 25 kg. A high-speed camera was used to see the deformation of the PSA layer. The impactors drop and hit an anvil connected to the lower end of the specimen, and impact occurred. The schematic of a specimen holder for the impact tests is shown in Fig. 2.19. [39].

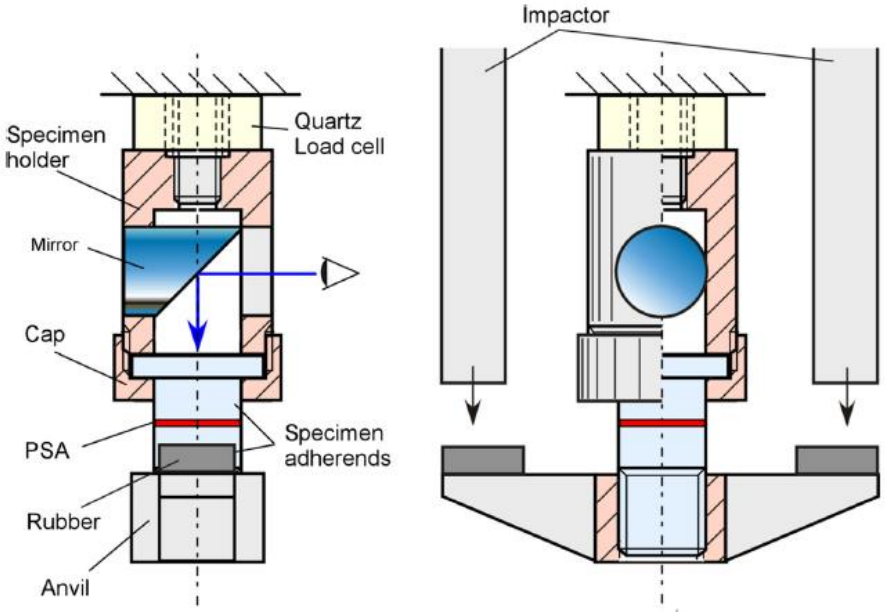

Figure 2.19 *Schematic of specimen holder for impact tests.*

Machado et al. have studied the impact behavior of the mixed joint in the single lap joint using stiff and flexible adhesives. The flexible adhesive is placed in the ends of the joint overlap to smoothen stress concentrations, while the stiff adhesive is put in the middle of the joint. Impact tests were performed with a drop-weight machine to obtain the best properties of the joint than the two adhesives individually. [40].

Chapter 3 : Numerical Simulation of Adhesive Butt Joint

This work aims to innovate a suitable geometry and setup for the medium velocity impact test for the adhesive joint. The specimen has been designed as a single and double adhesive butt joint to be tested with a standard drop dart testing machine. The proposed solution is achieved by a lot of research and development that can be easily applied with a variety of materials, as adhesive joints are used widely in industries nowadays. The numerical simulation is done before to achieve a possible geometry so that that the joint can fail in the failure mode II i.e., in shear but changing the geometric parameters means the dimensions can give either mode II failure or the mixed-mode implies a combination of both the mode I and mode II.

Instead of testing the bulk material testing, the adhesive joint would be better to evaluate not only the cohesive failure but also the adhesive failure and simulate the adhesive joints used in the industry. Therefore, before doing the impact test on the drop dart machine, the quasi-static test is performed to characterize the adhesive material. The adhesive butt joint geometry is shown in fig 3.1.

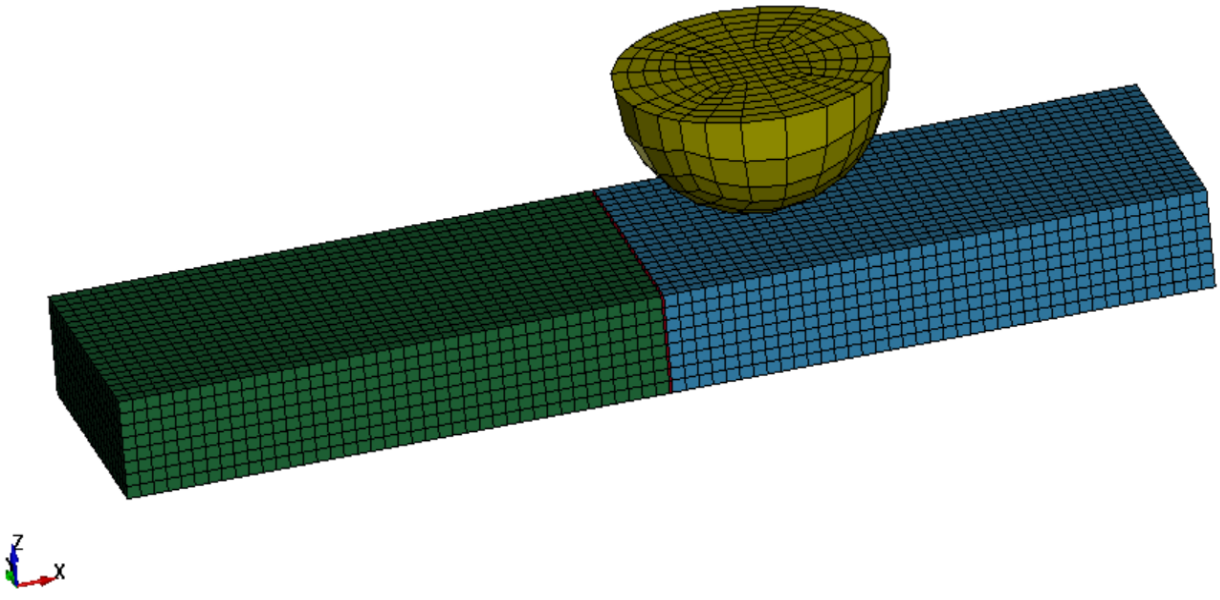

Figure 3.1 *Numerical model of single butt adhesive joint*

There are quite a lot of advantages of numerical simulation. One of them is saving money and time while doing several tests with different loading and boundary conditions. And the other is that at the same time, it is possible to intensely study the stress-strain response of the material with quite a good accuracy, accelerating several the geometric optimization to obtain the desired objectives. So, for example, using Ls- Dyna, it beneficial to test different material models for the substrate like for steel and the composite is used, while also varying the geometrical dimensions of the model.

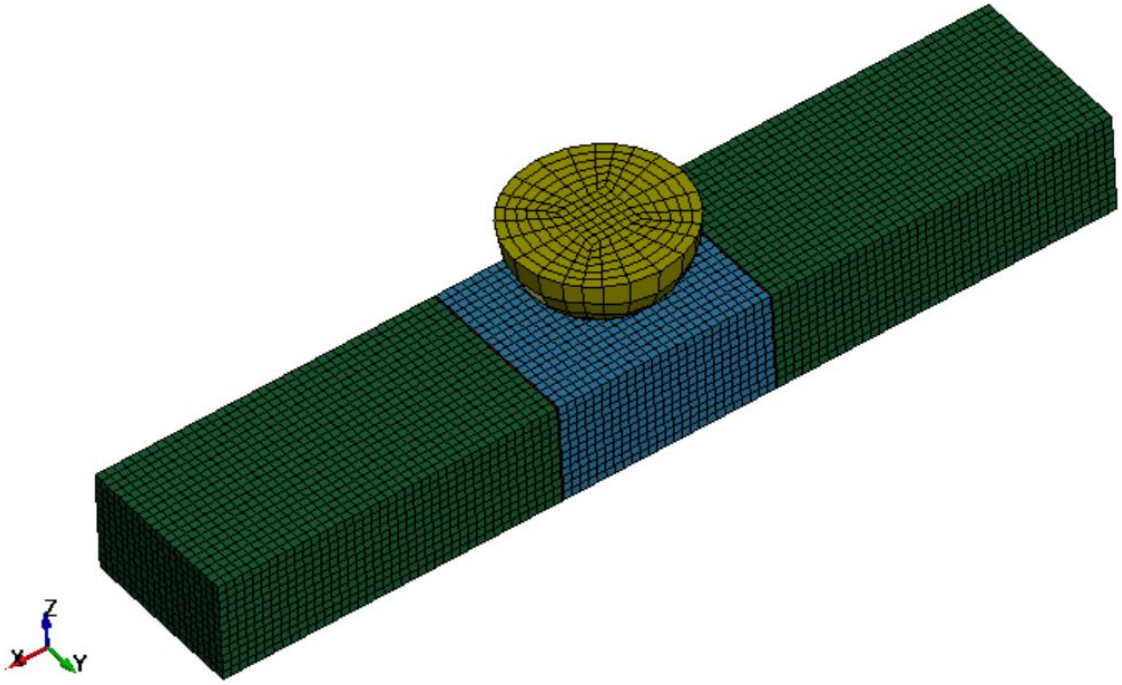

Figure 3.2 *Numerical model of double butt adhesive joint*

3.1 Development of the Numerical model

As mentioned above, this was a parametric study. Therefore, instead of developing the numerical model with different parameters (dimensions, mesh size, material properties, boundary conditions, impact parameters) repeatedly, the programming language named "Python" is used. The advantage of using Python is that it is a free source and is easy to learn. The script of the python can be found in Appendix 1.

The model has been achieved with a python script that operates another software that is a mesh generator (cf. https://gmsh.info/). Creates the mesh of the joint components and assembles all components in a keyword file (.k file) with all the required keywords for the model and post-analysis.

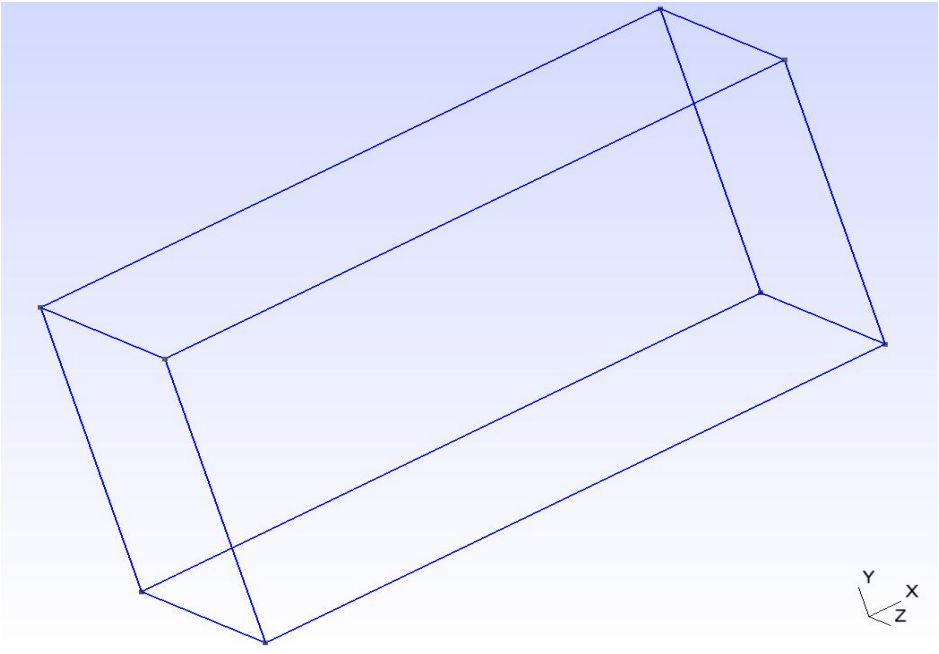

Figure 3.3 *Geometry of one of the adherends in GMSH software.*

As it is the advantage of the LS-Dyna that user can define their model with units whatever he is confident with, so the units used in this work are consistent from the beginning of the work, i.e., during the python script the post-processing of the model.

Parameters	Units
Dimensions	Mm
Weight	tons
Time	seconds
Energy	J
Stress	MPa
Force	N

Table 3.1 *Units used in the model.*

3.2 Adherend Specifications

3.2.1 Material Used

The adherends used for the test are made up of carbon fiber with a twill weave pattern and steel. The elements used for the adherends are solid elements and very compatible with the material that was used. Two material models are adopted for these substrates.

*Mat 003/*Mat Plastic Kinematic: For the steel material

Mat 059/ Mat_Composite_Failure_Solid_Model: For the composite material, carbon fibers twill weave.

This model is suited to model isotropic and kinematic hardening plasticity with the option of including rate effects; also, it is a very cost-effective model and is available for beam (Hughes-Liu and Truss), shell, and solid elements. [20]. This material model is used because the deformation of adherends is minimal and plastic strain has to be avoided. The parameter ETAN (Tangent modulus) is used in this model: the slope of the bilinear stress-strain curve.

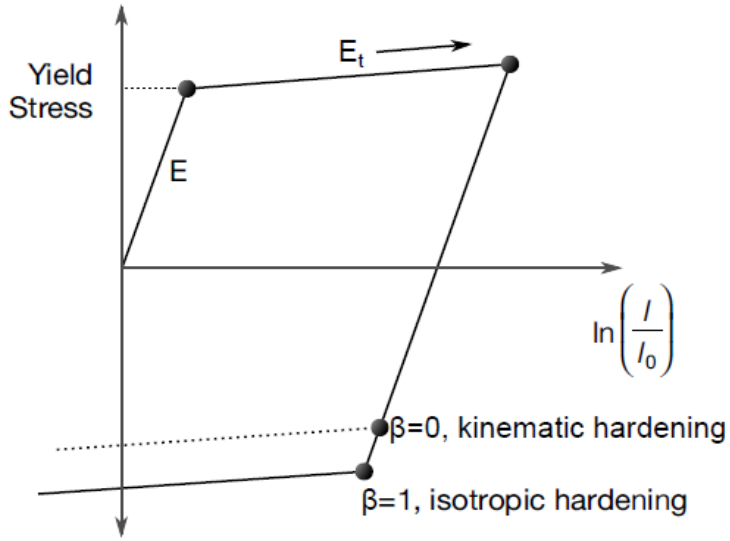

Figure 3.3 *Elastic-plastic behavior with kinematic and isotropic hardening [20]*

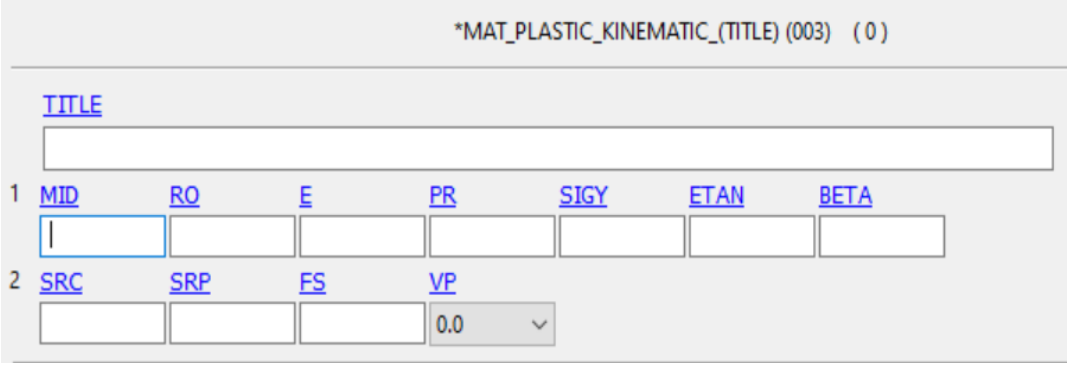

Figure 3.4 *Parameters required for the Mat_ Plastic_Kinematic*

Where;

MID: It is the material identification number.

RO: is the density of the material

E: Young's Modulus

PR: Poisson's Ratio

SIGY: Yield stress

ETAN: Tangent Modulus

Beta: Hardening parameter, $0 < \beta' < 1$.

SRC and **SRP**: Strain rate parameters C and P for Cowper Symonds strain rate model. And in this study, they are zero means they are not considered.

FS: Effective plastic strain for eroding elements.

Parameters	Values
Density, ρ [Ton/m^3]	7.8
Elastic Modulus, E [MPa]	200×10^3
Poisson's Ratio, ν [-]	0.3
Yield Stress, σ_y [MPa]	170
Tangent Modulus, E_{tan} [MPa]	821.5
Effective plastic strain, ε_f [-]	28%

Table 3.2 *Mat 003 material card for DD11 steel.

Only kinematic hardening has been considered in this model. The material studied is the DD11 steel, very low carbon, and hot rolled steel for plastic deformation, usually used for deep drawing. It has a low yield strength and excellent formability.

Mat 059/* Mat_Composite_Failure_Solid_Model: For the composite material carbon fibers.

Material type 59 in Ls-Dyna is intended to capture the damage in composite materials. This model is based upon the damage model described by Cheng and Hallquist [41] and incorporates 8 failure modes, which are

- Mode1: Tensile longitudinal (material 1 direction) fiber failure
- Mode2: Transverse (material 2 direction) tensile failure
- Mode 3: Through-thickness (material 3 direction) shear (combined with longitudinal tension)
- Mode 4: Delamination
- Mode 5: Through-thickness shear (combined with transverse tension)
- Mode 6: Longitudinal compressive failure of the fibers
- Mode 7: Transverse compression
- Mode 8: Through-thickness compression

All the formulas for this type of model are attached in the Appendix II.

The material model is relatively easy to use as it is a stress-based model, and it does not include the strain rate effect because, in this study, the main concern is for the adhesive material. When type Mat 059 is used with solid elements, as it was in this case, this model can check for delamination effects by observing matrix failure in the through-thickness direction.

Other material models are also available in Ls-Dyna using different laminate failure criteria suggested by Tsai and Wu. Still, these criteria were only available for shell elements. Therefore, mat 059 with solid elements was chosen to simulate delamination, and it is easy to use. However, this model is more computationally expensive to run than mat 003, the one used for steel adherends. But has the advantage of incorporating orthotropic properties, as the composite materials are orthotropic. Furthermore, the fiber directions are established, and fiber failure properties are different in compression and tension.

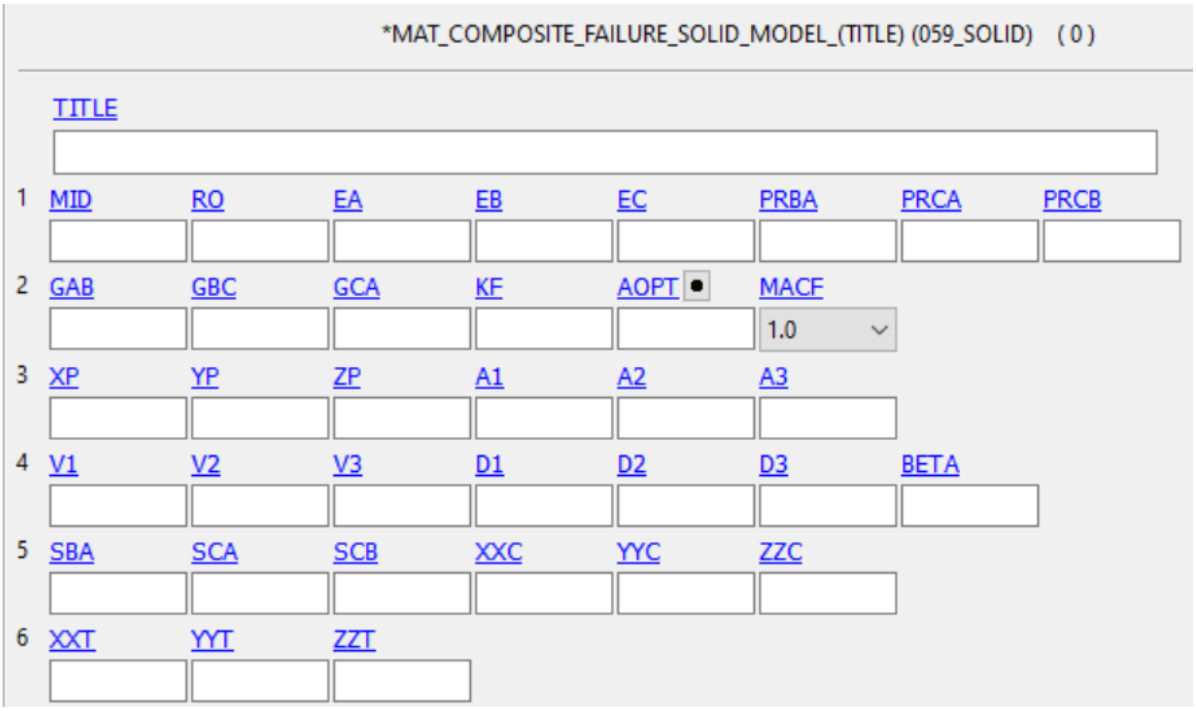

Figure 3.5 *Parameters required for the Mat_Composite_Failure_Solid_Model*

Where;

EA = Elastic Modulus in a (longitudinal) direction

EB = Elastic Modulus in b (transverse) direction

EC = Elastic Modulus in c (transverse through the thickness) direction

PRBA = Poisson's ratio in ba direction

PRCA = Poisson's ratio in ca direction

PRCB = Poisson's ratio in cb direction

GAB = Shear stress in the ab direction

GAB = Shear stress in the ab direction

GBC = Shear stress in the bc direction

GCA = Shear stress in the ca direction

AOPT: Material axes option its value is from 1.0 to 4.0.

EQ.2.0: Globally orthotropic with material axes determined by vectors defined below, as with *Define_Coordinate_Vector.

SBA = In-plane shear strength

SCA = Transverse shear strength

SCB = Transverse shear strength

XXC = Longitudinal compressive strength x-axis.

YYC = Transverse compressive strength b-axis.

ZZC = Normal compressive strength c-axis.

XXT = Longitudinal tensile strength a-axis.

YYT = Transverse tensile strength b-axis.

ZZT = Normal tensile strength c-axis.

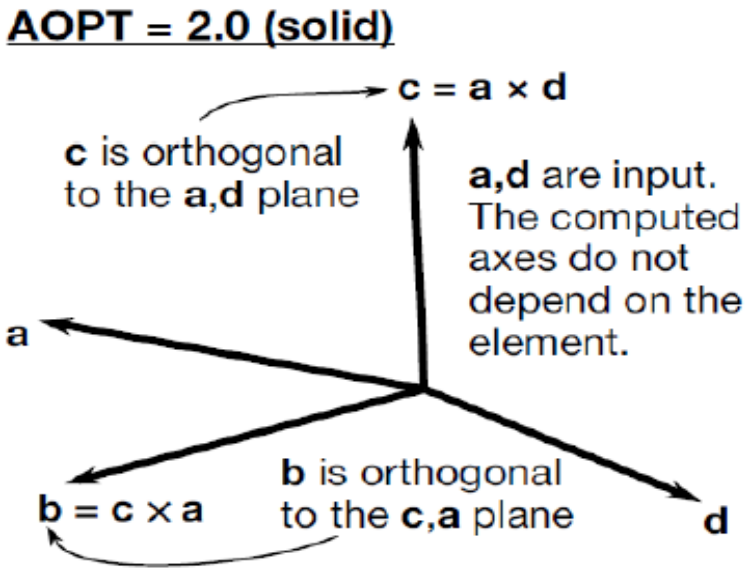

Figure 3.5 *Two vectors a and d are defined, and the triad is computed and stored.*

This model is suitable for unidirectional composite layers, complete laminates, and woven fabrics. In this work, it was applied to simulate a carbon fibers composite laminate with an epoxy matrix. This material was used in the experimental tests; the specimen was 20mm wide and 7.04 mm thick with 8 layers with a 0/90 stacking sequence. The main mechanical properties are reported in table 3.2.

Parameters	Values
RO, ρ [kg/m^3]	1.5×10^{-9}
EA, E_a [MPa]	5.4×10^4
EB, E_b [MPa]	5.4×10^4
EC E_c [MPa]	5.4×10^2
PRBA, ν_{ba} [-]	0.08
PRCA, ν_{ca} [-]	0.08
PRCB, ν_{cb} [-]	0.08
GAB, G_{ab} [MPa]	3500
GBC, G_{bc} [MPa]	3500
GCA, G_{ca} [MPa]	3500
SBA, τ_{ba} [MPa]	84
SCA, τ_{ca} [MPa]	84
SCB, τ_{cb} [MPa]	84
XXC,$\sigma_{a'}$ [MPa]	520
YYC, $\sigma_{b'}$ [MPa]	520
ZZC, $\sigma_{c'}$ [MPa]	200
XXT, σ_a [MPa]	800
YYT, σ_b [MPa]	800
ZZT, σ_c [MPa]	260

Table 3.3 *Mat 059 material card for carbon fiber with epoxy laminate.*

3.2.2 Element type used

For steel material, element type 2, which is a fully integrated solid, can be used. It is a particular reduced integrated brick element, and no hourglass stabilization is required, but it has a problem that it is slower than element type 1 (elform = 1). In addition, the elform = 2 is unstable for large deformation as the steel is not very flexible compared to the composite carbon fibers, so that it can be used for the steel.

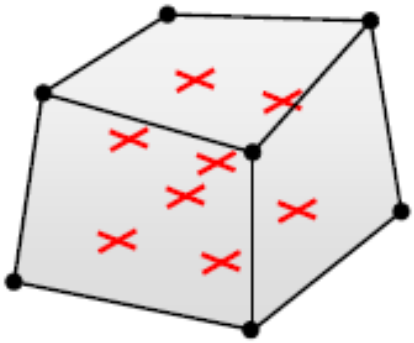

Figure 3.6 *Element formulation type 2*

For composite material, element formulation 1, which is constant stress solid element which is a default element type used in the Ls-Dyna. It is under integrated constant stress, works for severe deformations, also efficient and accurate, but hourglass stabilization is required. There is quite a lot of research done on the type of hourglass formulations and their values. For stability purposes in bending loading conditions, hourglass energy has to be activated in Ls-Dyna. However, it has been limited to 5% of the total energy, so it may not affect the results much.

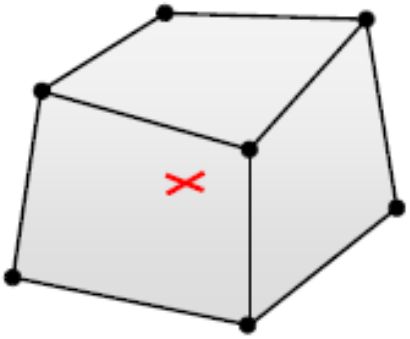

Figure 3.7 *Element formulation type 1*

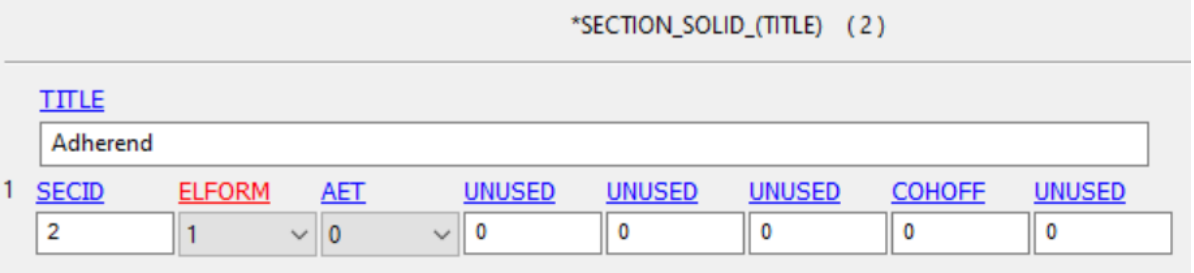

Figure 3.8 *Input Parameters of solid elements*

So, the element formulation type 1 (elform = 1) is used for both cases with the suitable type and value of hourglass. The material models' material card *mat 003 can be useable for both the shell and solid elements. Moreover, no adjustment or further analysis was required being this material isotropic, i.e.; it exhibits the same properties in all directions. Implementing the solid elements formulation for the composite material was a little bit complex than that of the steel. This execution was difficult without the support of dedicated material characterization. Typical in-plane material properties are provided by the laminate and composite fabrics suppliers. Only the matrix can bear the load in laminates subjected to load in the transverse direction orthogonal to the fibers. The mesh shape used is the 3-D solid element, and the mesh size is 1mm in the horizontal order and 1mm in the vertical direction.

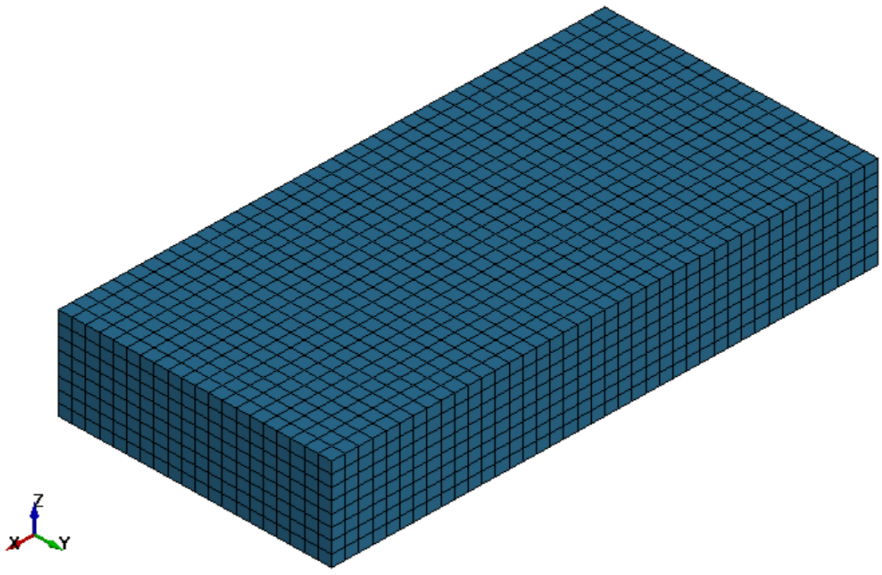

Figure 3.9 *Adherend after meshing.*

3.3 Adhesive Specifications

3.3.1 Material Used

This research focused on the two adhesive materials: one is stiffer, epoxy, and the other is flexible polyurethane. As mentioned in **section 2.5,** there are three ways to model the adhesive material; the one used a lot and was focused on is the cohesive zone model (CZM), and the material model was used is the mat_138 (Mat_Cohesive_Mixed_Mode). It is a simplified bilinear characteristic. It produces effective results with epoxy and other structural adhesives of interest of a test like this; anyhow, the main aspects of this keyword have already been illustrated in **section 2.5.1**. Further advancement in this feature would be implementing a more complicated material model like mat 240, which can also investigate the strain rate sensitivity of the adhesive material.

The research has been focused on two materials, whose cards are shown in table 3.3. First, the material properties of the polyurethane adhesive have been chosen from experimental data of tests performed via the single lap joint tests by the research group[1] of the Polito under Prof. Goglio's supervision. The SLJ test was performed at a speed of 2mm/min. The test was performed on similar and dissimilar substrates: CFRP/CFRP, PMS/PMS, and CFRP/PMS, with two different overlap dimensions, 12 mm and 24mm. [42]. Second, the epoxy's material properties have been chosen to start from the experimental data of the Arcan test performed in tensile, shear, and 30, 45, 60 degrees loading conditions. All the data have been interpolated with the mat_138 (Mat_Cohesive_Mixed_Mode) bilinear characteristic and further corrected via an Ls-Dyna numerical simulation of the same test. In the adhesive modeling, if the shell elements are the chosen contact keyword: tied shell edge to surface constrained offset, which is suitable for cohesive elements, it can transmit forces and moments. But in this work, solid element formulations are used, so there is no need to define tied contact. Furthermore, the coupled nodes have been merged even though if it is specified, then it will not affect the results obtained from the numerical simulation.

[1] J-TECH@POLITO

(Advanced Joining Technologies at Politecnico di Torino)

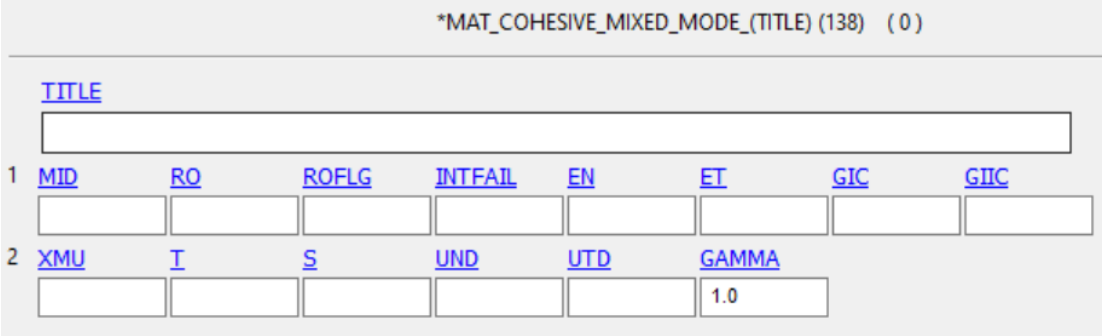

Figure 3.10 *Parameters required for the Mat_Cohesive_Mixed_Mode*

Where;

RO = Mass density.

ROFLG = Flag for whether density is specified per unit area or volume. Roflg=0 specified density per unit volume (default), and Roflg=1 specifies the density is per unit area for controlling the mass of cohesive elements with an initial volume of zero.

INTFAIL = The number of integration points required for the cohesive element to be deleted. If it is zero, the element will not be deleted even if it satisfies the failure criterion. The value of INTFAIL may range from 1 to 4, with 1 the recommended value.

EN = The stiffness normal to the plane of the cohesive element.

ET = The stiffness in the plane of the cohesive element

GIC = Energy release rate for mode I.

GIIC = Energy release rate for mode II

XMU = Exponent of the mixed-mode criteria

T = Peak traction in a normal direction

S = Peak traction in a tangential direction

UND = Ultimate displacement in the normal direction

UTD = Ultimate displacement in the tangential direction.

GAMMA = Additional exponent for Benzeggagh-Kenane law (default = 1.0)

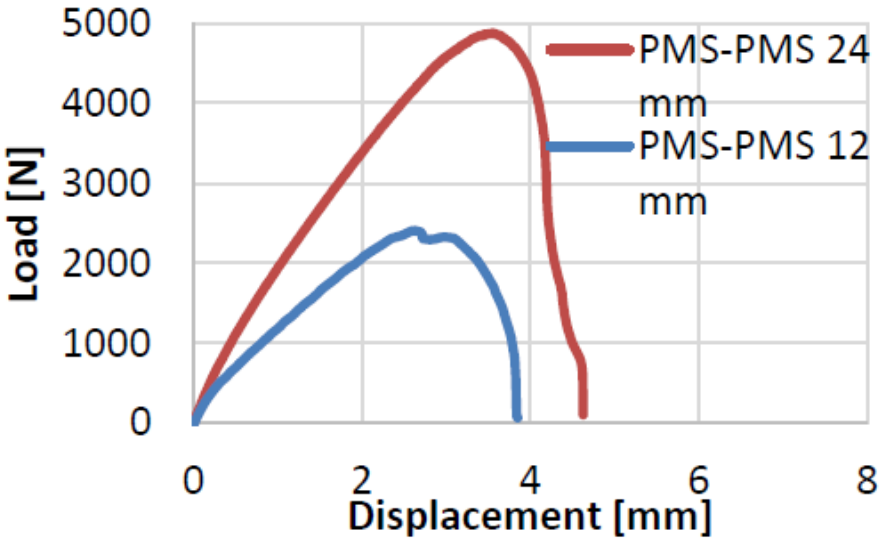

Figure 3.11 *Load- displacement curve of SLJ Test on the PMS substrates [42]*

PMS – PMS 24 mm = Painted metal substrate with an overlap of 24 mm.

PMS – PMS 12 mm = Painted metal substrate with an overlap of 12 mm.

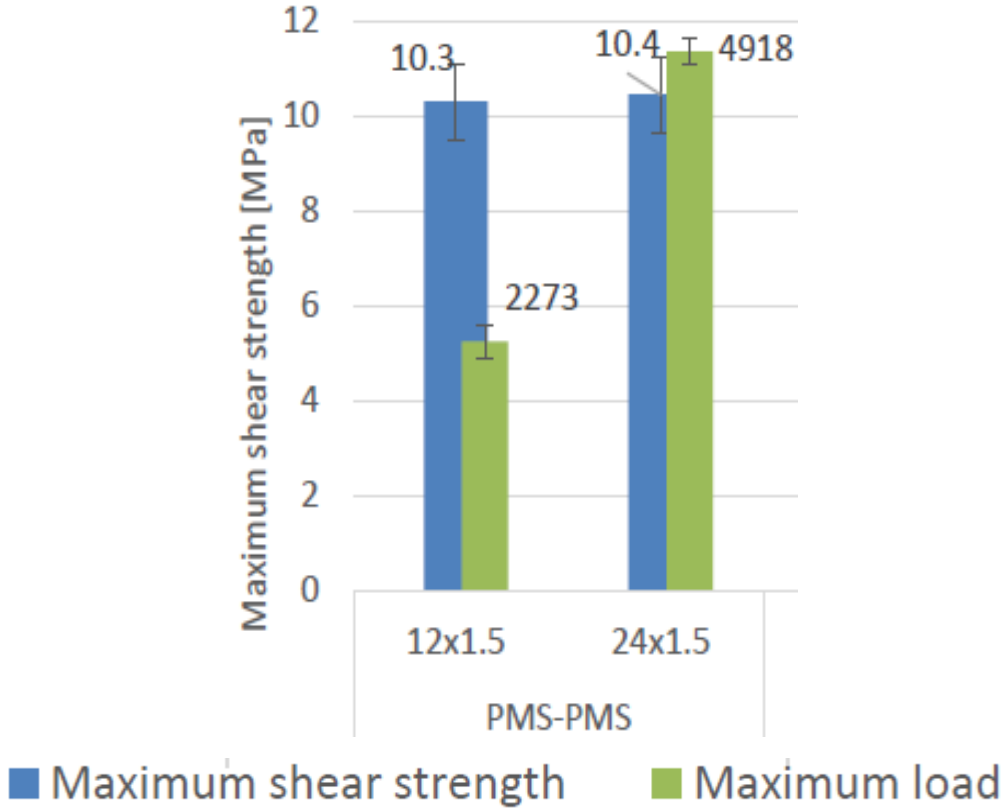

Figure 3.12 *Result of the SLJ tests [42]*

Parameters	Values
RO, ρ [Ton/m^3]	0.98
EN, E_n [MPa/mm]	3.214
ET, E_t [MPa/mm]	3.214
GIC, G_{IC} [MPa. mm]	5.975
GIIC, G_{IIC} [MPa. mm]	23.9
T, σ_t [MPa]	5.0
S, σ_s [MPa]	10.0
UND [mm]	2.39
UTD [mm]	4.78
XMU [-]	2

Table 3.4 *Mat 138 material card for Polyurethane adhesive.*

Parameters	Values
RO, ρ [Ton/m^3]	1.22
EN, E_n [MPa/mm]	8.0801
ET, E_t [MPa/mm]	13.8175
GIC, G_{IC} [MPa. mm]	3.4159
GIIC, G_{IIC} [MPa. mm]	8.164
T, σ_t [MPa]	7.1913
S, σ_s [MPa]	13.9556
UND [mm]	0.95
UTD [mm]	1.17
XMU [-]	1

Table 3.5 *Mat 138 material card for Epoxy adhesive.*

The linearity both in the loading process and in the softening process provides a simple relation for the two energy release rates:

$$G_{IC} = T \times \frac{UND}{2}$$

$$G_{IIC} = S \times \frac{UTD}{2}$$

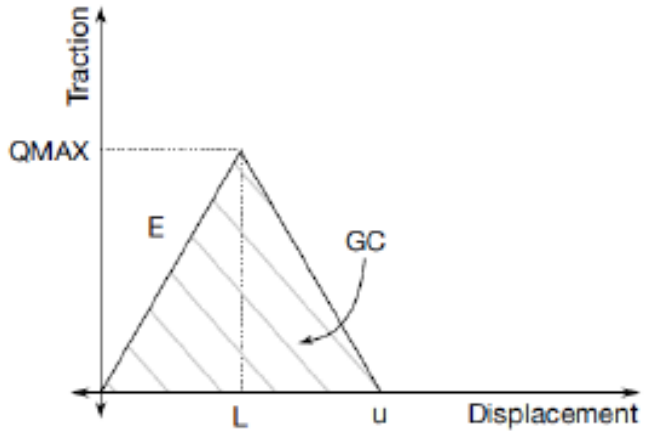

Figure 3.13 *Bi-linear traction separation law for Mat_138*

3.3.2 Element type used

For the adhesive material, the element formulation of type 19 is used. It is an 8 – noded, 4-point cohesive element. The tractions on a mid-surface are described as the mid-points between the nodal pairs 1-5, 2-6, 3-7, and 4-8. These are functions of the differences of the displacements between nodal pairs interpolated to the four integration points. The initial volume of the cohesive elements may be zero; in that case, the density can be defined in terms of the area of nodes 1-2-3-4, and the tractions are calculated in a local coordinate system defined at a centroid of an element.

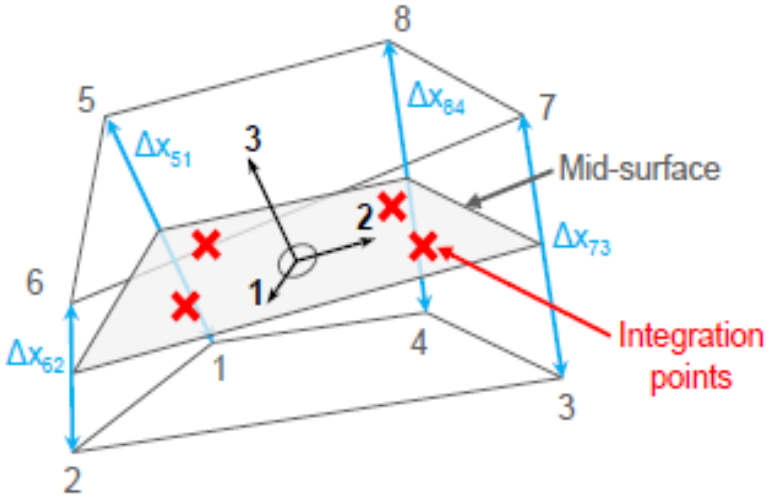

Figure 3.13 *Illustration of solid local coordinates. [43]*

3.4 Boundary conditions and Impactor modeling

The boundary conditions include a set of clamped nodes of the adherends and a rigid cylindrical wall for each clamping side of the adherends. This is the schematization chosen for the clamping system of the dart impact test machine. The rigid walls have been placed to evaluate whether the radius of curvature of the fillet of clamping base has any effect on numerical results.

It was a parametric study to define the clamping of the adherend by different methodology by defining the box. Then, the area included by that box is clamped.

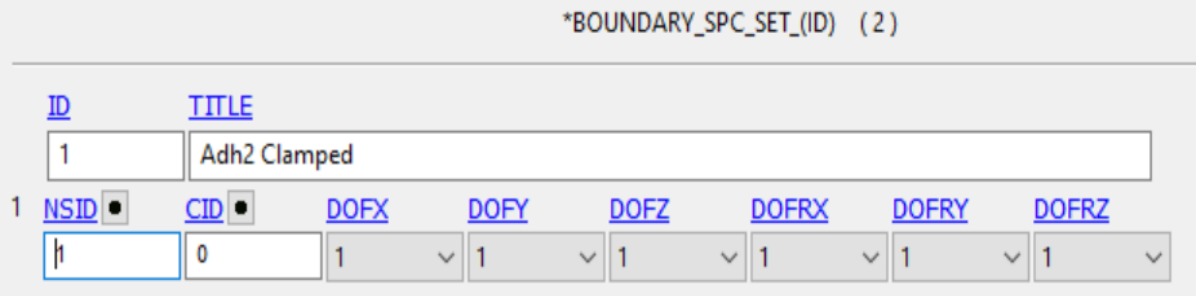

Figure 3.14 *Boundary condition for the adherend*

3.4.1 Material Used for Impactor

The impactor material is quite stiff and strong as during the test; it does not deform or damage, so for this case, in Ls-Dyna, it is model as the rigid material model.

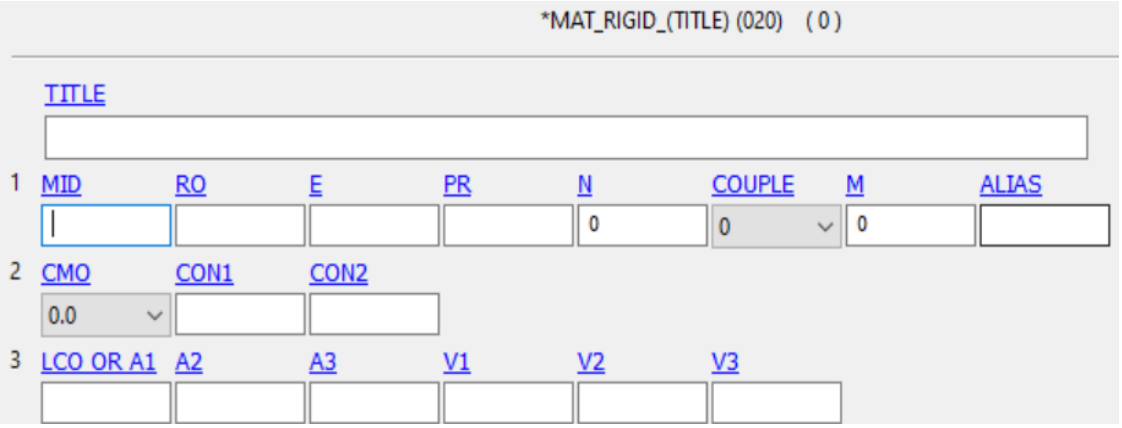

Figure 3.15 *Parameters required for Mat_Rigid*

Where:

RO:=Mass density.

E:=Young's modulus.

PR:=Poisson's ratio

M:=MADYMO/CAL3D Coupling option flag: EQ.0: use normal LS-DYNA rigid body updates.

Parameters	Values
RO, ρ [Ton/m^3]	4.97×10^{-7}
E [MPa]	210×10^3
PR, ν [-]	0.300

Table 3.6 *Mat 020 material card for Impactor.*

The impacting energy is provided to a rigid hemispherical body which is the impactor. The impactor velocity is set by an initial velocity condition, while the impacting mass is set with a calibrated density. Except for the z (vertical) direction all the other degree of freedom is a constraint of the impacting body. It can be noted that the rigid material may make the impact tougher. Still, it can be assumed that the machine is much stiffer than the tested specimen making this simplification acceptable.

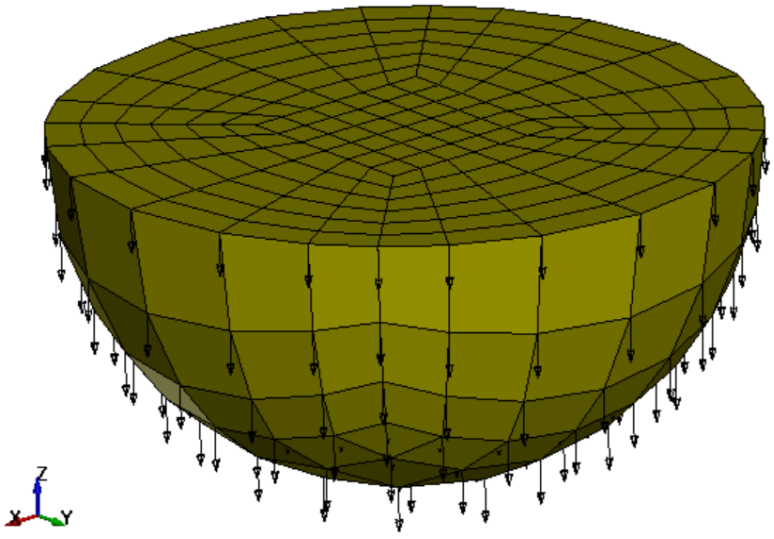

Figure 3.16 *Impactor assigned initial velocity to each node of the mesh.*

3.4.2 Element type used

The element used for the rigid impactor is element type 1 (elform = 1). As that impactor is not much of the research concern, using element type 1 reduces the required computational power and time, as was already mentioned in detail in section 3.2.3.

3.5 Output Set up

The necessary termination time is usually from 0.3 - 1.5 ms, while as control and post-analysis optional variables have been set the following keywords:

- Control Contact
- Control Hourglass
- Control Timestep
- Database ASCII Option
- Database Binary D3plot
- Database Extent Binary

In database_binary_d3lot, it was important to properly adjust the timestep according to the test duration or velocity so that the data were recorded with consistent resolution.

The control hourglass type 4, eq.4: stiffness form of type 2 (Flanagan-Belytschko) is used because for the adherend type 1 (elfrom =1) is adopted. So, it is obligatory to use a control hourglass for the accuracy of the numerical results. The value was 0.03 as the hourglass energy is less than 5-10 % of the total energy. Without hourglass control, these elements would have zero energy deformation modes which could grow large and destroy the solution.[43].

3.5.1 Database_Rcforc

LS-Dyna can write a lot of possible output files concerning the contact. The first one used in this project is called database_rcforc, an ASCII file containing resultant contact forces for both the slave and master sides of each contact interface.

3.5.2 Database_Spcforc

With this card is possible to compute the force involved in the elements where a constrained boundary condition is imposed.

3.5.3 Database_Secforc

To double-check the forces in the contact region, one more ASCII file can be written by using the ’database_secforc’ keyword. The latter needs a reference plane to define the area where the force and moment must be computed.

Chapter 4 : Results

The Ls-Dyna model was useful to optimize the joint configuration and provides some fascinating results that are not easily obtained from the experimental tests, like the substrate bending deformation that significantly affects the test behavior. Moreover, some analyses are impractical or difficult to be performed on experimental data. For example, the stress-displacement field of the cohesive elements and the crack initiation and propagation analysis, but nowadays, thanks to high-speed cameras, can also analyze crack initiation and propagation in the experimental test.

4.1 Single Butt Joint

This type of adhesive joint is tested for three configurations, the impacting dart is far away from the adhesive, the second is dart away from adhesive, and the last is dart near adhesive.

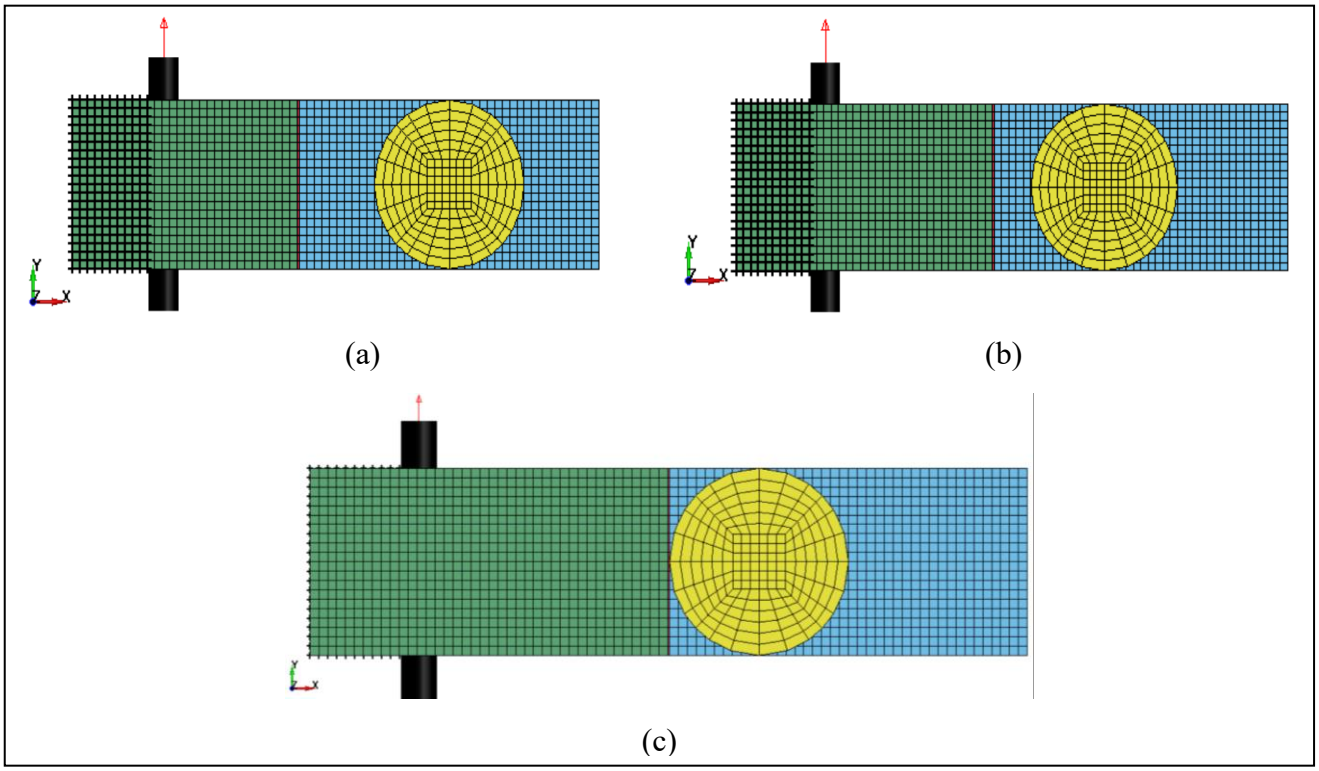

Figure 4.1 *Three configurations of the single butt joint. (a) dart impacting far away from the adhesive, (b) dart impacting away from the adhesive, and (c) dart impacting near adhesive*

As seen from the results, if the thickness of adherends is less, there is quite a lot of vibration in adherends, which are clamped. So, that may produce a distortion in the obtained results; that is why the thickness of the clamped adherend should be at least greater or equal to the 7 mm. Therefore, in this study, the thickness of the steel adherend is chosen to be 12 mm.

From the three-configuration shown in ***figure 4.1,*** the (c) configuration is better than the other two in the sense of the failure in the 2nd mode because as the dart moves away from the adhesive, it increases the bending moment adhesive is placed. As a result, it will produce peel stress in the system. As a result of these peel stress, shear stress present in the beginning decreases when the dart impacts and the adhesive fail not only in mode II but in mixed mode. As a result, the adhesive will fail in the 2nd mode and the mixed mode. Achieving a shear load in this specimen, the impactor must be hit just beside the bond line. [22]. So, the configuration (c) is better than the other two configurations; this configuration is simulated with a different material model. A similar type of results was seen while using steel, composite adherends with polyurethane and epoxy adhesive.

1. Steel Substrate with Polyurethane Adhesive
2. Steel Substrate with Epoxy Adhesive
3. Composite Substrate with Polyurethane Adhesive
4. Composite Substrate with Epoxy Adhesive

4.1.1 Dimensions of the Specimen:

Parameters of the adhesive material are the following:
Adhesive width: 20 mm (along the y-direction)
Adhesive thickness: 0.2 mm;

Parameters of the adherend material are the following:

Adherend width is the same as that of the adhesive, i.e., 20 mm

Adherend thickness: 12mm

During the study, the length of adherend 1 is fixed (the blue one in **figure 4.1**) 40 mm and changing the length of the adherend 2 (green in **figure 4.1**) 30mm, 35mm, and the 40mm cases to achieve the three configurations mentioned above.

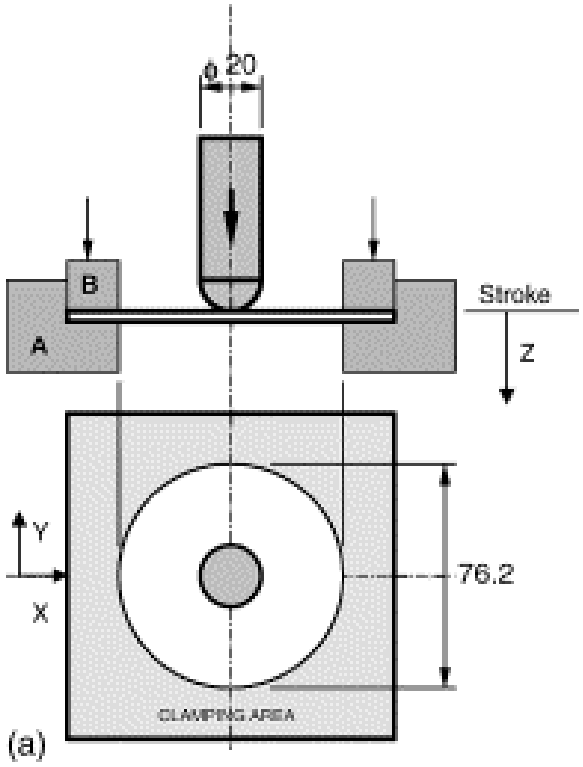

Figure 4.2 *Clamping dimensions of the Dart Impact Machine*

As the trend of all the material models mentioned in **section 4.1** similar, the result presented here was only with the case of the Steel Substrate with Epoxy Adhesive with the configuration (c).

4.1.2 Steel Substrate with Epoxy Adhesive

The epoxy adhesive is relatively stiffer than that of the polyurethane. Therefore, the impactor's kinetic energy is constituted of two terms: one is the mass and the other is the velocity; the mass is kept constant, i.e., 1 kg as the velocity is increased, so the kinetic energy is increased.

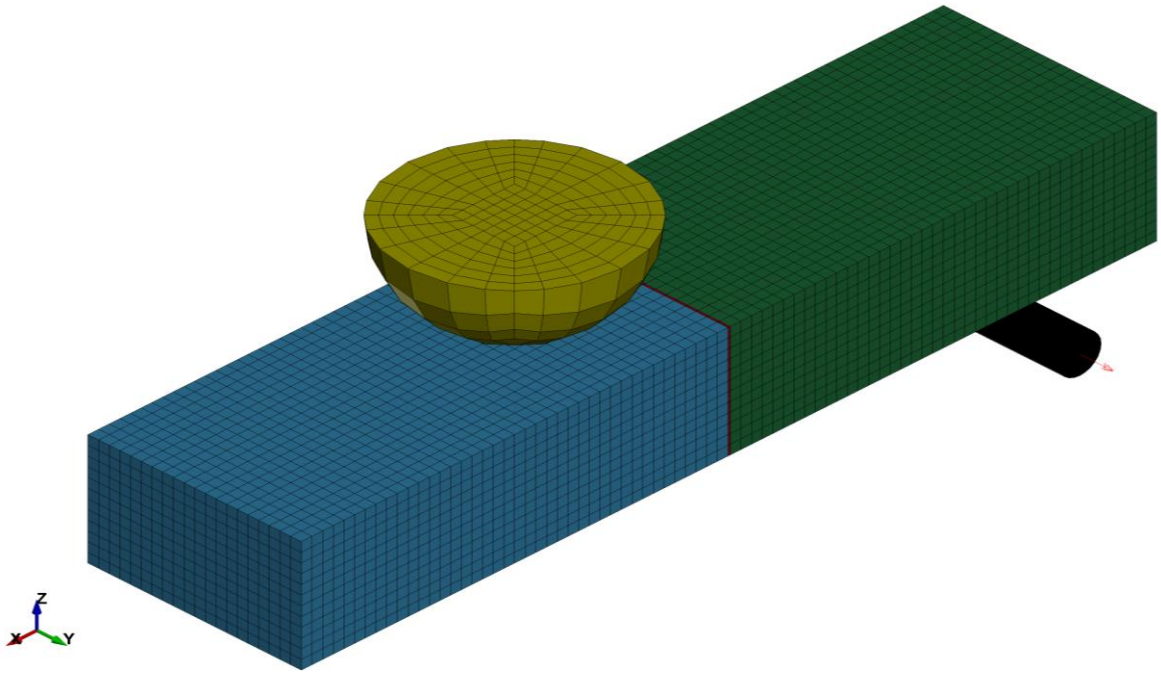

Figure 4.3 *Numerical model of single butt joint with configuration (c)*

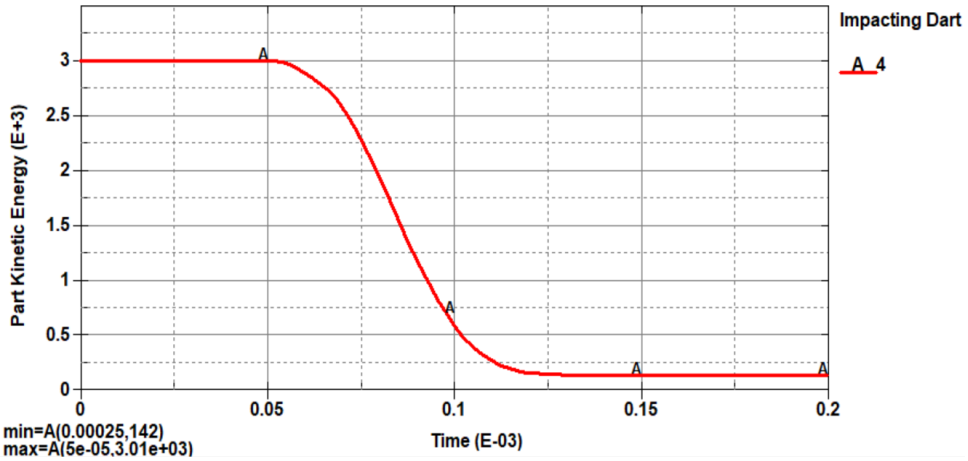

Figure 4.4 *Kinetic Energy of the Impacting Dart at Low energy (low velocity)*

It is evident from figure 4.4 that energy provided to the dart, almost all the energy is absorbed by the adhesive. The restituted energy on the dart is relatively low in the order of 0.3J. The kinetic energy is reported in $\left(tons \times (mm)^2 / (s)^2\right)$, which is the 3J, it was observed from the results that the 3J is enough energy that can break the joint, but the failure obtained was not only due to the shear stresses, but it was the combination of both failure modes, i.e., mode I and mode II.

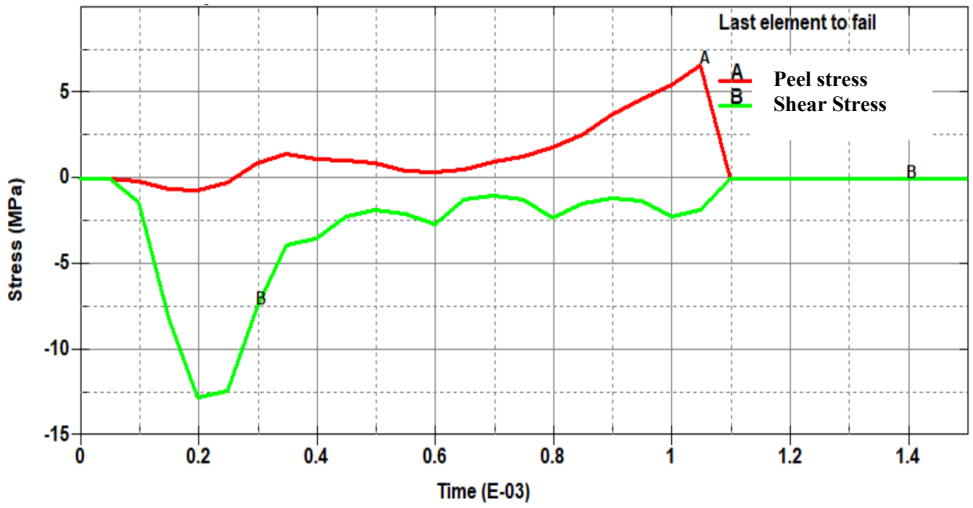

Figure 4.5 *Stress vs time plot of last adhesive element to fail at low energy (2.5 m/s).*

The stress induces at the beginning of the test was shear. As the dart progress downwards, it introduces the peel stresses in the adhesive and just before the failure as it is not failing due to mode II only, but due to the combination of the mixed-mode mean of mode I and mode II.

But when the velocity was increased up to 6.8 m/s, then the adhesive was failing only in the 2nd mode, i.e., only due to the shear stresses, the energy supplied to the impactor is 23J, as it can be seen in **figure 4.6**.

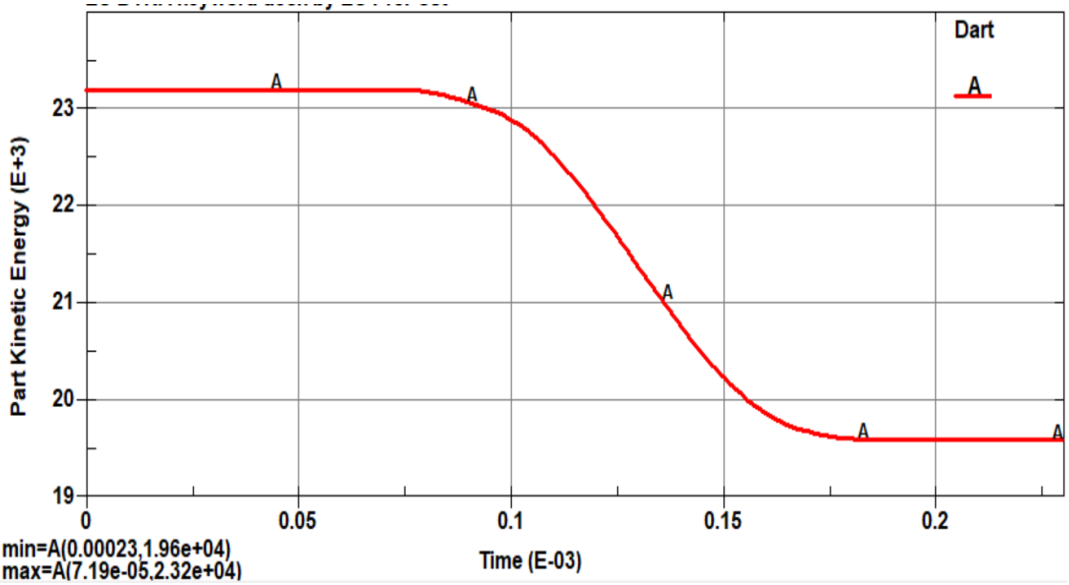

Figure 4.6 *Kinetic Energy of the Impacting Dart at the high energy (high velocity)*

These types of results are dynamic ones there are due to the inertial effect. As it can be seen from **figure 4.7** that the z- displacement (which is the vertical axis) node 6 is the node of the adherend which is near to the adhesive, while node 552 is on the other end of the adherend which is free.

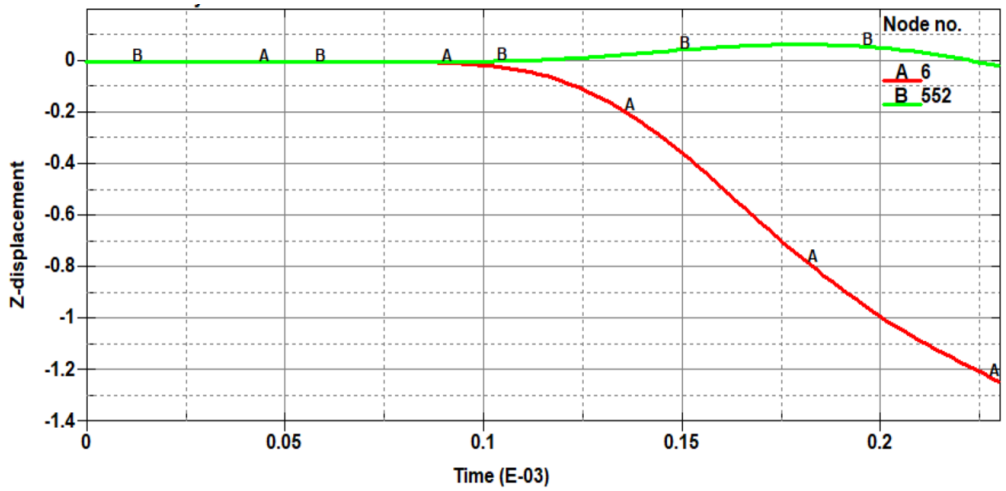

Figure 4.7 *Vertical displacement of the nodes at high velocity 6.8 m/s.*

As it can be understood from **figure 4.7** that the results high dynamic mean the part of the adherend which is near to adhesive when adhesive failed it has the displacement of 1.2 mm but the part of the adherend which was free and still have the zero displacements. But if the difference between the dart's impacting energy before failure and after failure, the amount of energy absorption is the same, 3.4J.

4.1.2.1 Crack propagation

The first element to fail was due to shear stresses only, but as the damage progress to the last element, the adhesive was failing due to both shear and peel stress as it can be seen in the above figure 4.6, the stresses in the red are the peel stresses, but the stresses in the green are the shear stresses. This is because damage propagates from the top of adhesive layer till the bottom of the adhesive, so it can be said that crack is propagating from top to bottom.

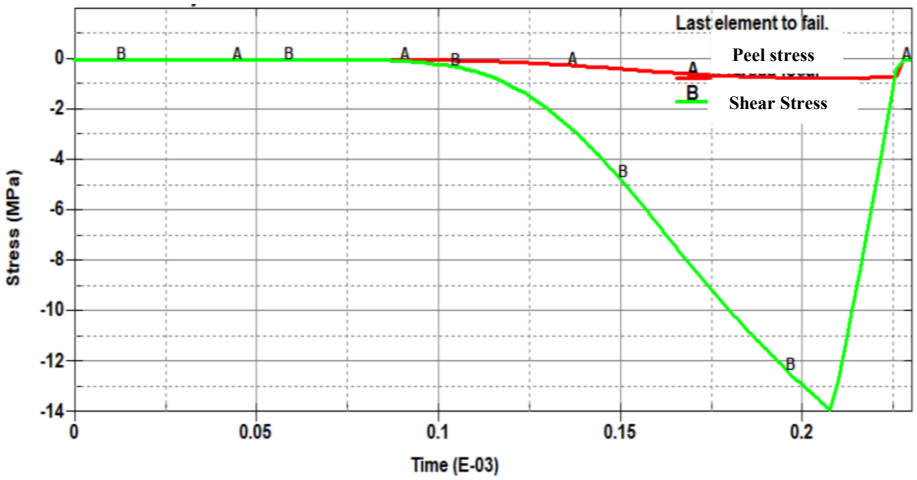

Figure 4.8 *Stress vs time plot of last adhesive element to fail at 6.8 mm/s.*

As shown from the results, failure was only due to the 2nd mode because stress obtained was only due to the shear stresses, but all the elements were failing at the same time, so if the stress vs time is plotted for all the elements, it is almost similar.

4.2 Double Butt Joint

In this joint, there are three adherends, and there are two layers of adhesive material used to bond these three adherends. For the double butt joint, two types of adherend materials are steel and the other is carbon fiber twill pattern composite material.

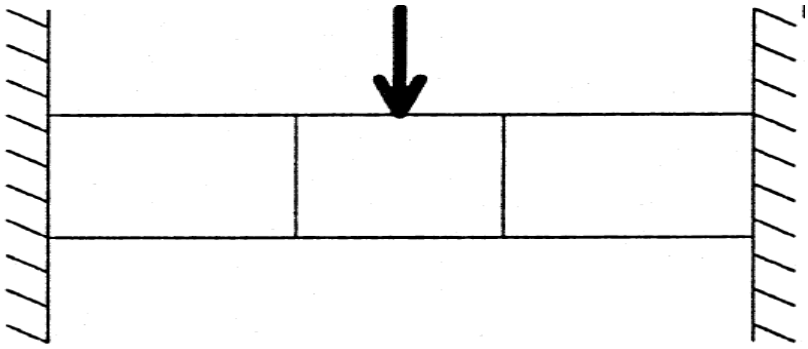

Figure 4.9 *Schematic of double butt adhesive joint [22]*

4.2.1 Steel Substrate with Polyurethane Adhesive

Parameters of the adhesive material are the following:

Adhesive width: 20 mm (along the y-direction)

The adhesive thickness on both sides: 0.2 mm;

Adhesive material: Polyurethane

Parameters of the adherend material are the following:

Adherend width is the same as that of the adhesive, i.e., 20 mm

Adherend thickness: 12mm

Adherend material: DD11 steel.

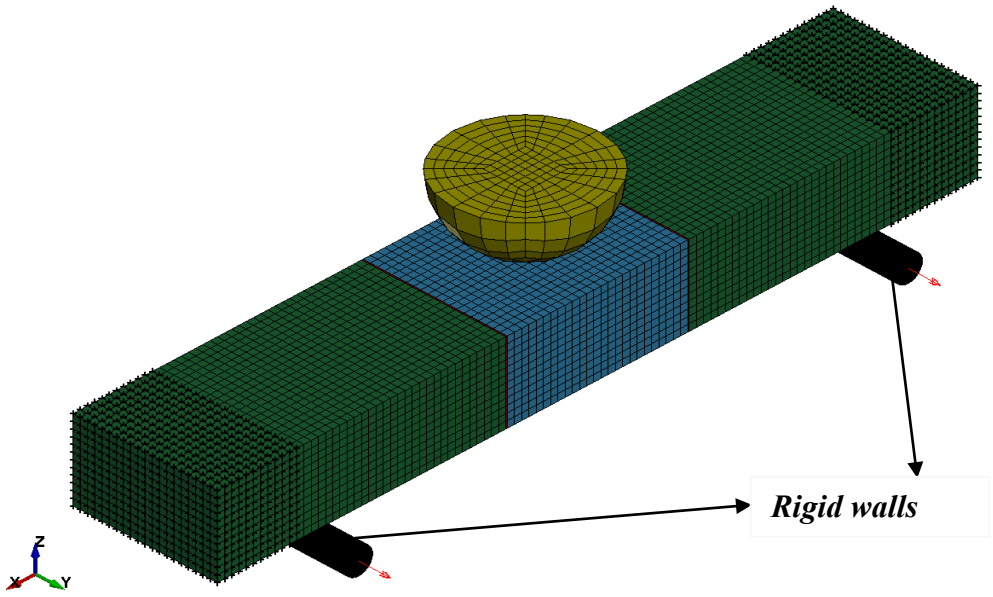

Figure 4.10 *Numerical model of the double butt adhesive joint.*

The middle adherend is the blue one since if different materials are to be adhesively bonded so the same type of model can be used, just by changing the material of the middle adherend. The two green adherends are clamped, as shown in **figure 4.10.** As the model is balanced in the sense that both adhesive layers failed simultaneously, there was no problem with the eccentricity of the load. The velocity of the dart is 4.8 m/s, and the impact energy is 11J which can be seen from fig 4.11.

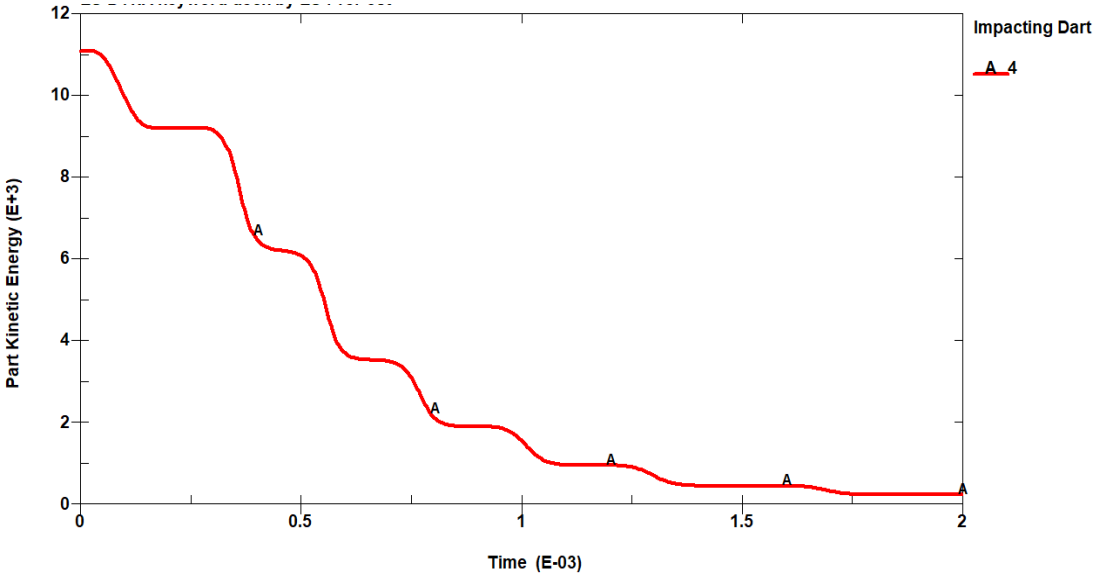

Figure 4.11 *Kinetic Energy of the impact dart for steel double butt joint*

4.2.1.1 Stress Analysis

In the double butt joint, there is no any dynamic effect. There are only the shear stresses which are present in the adhesive layer.

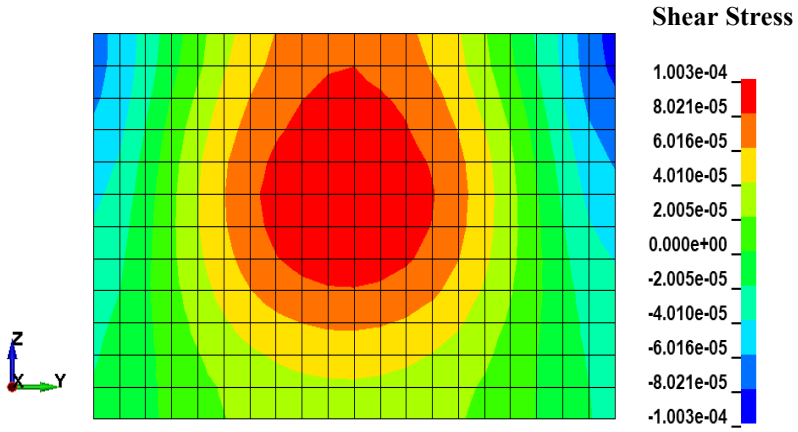

Figure 4.12 *Distribution of the shear stresses in the adhesive as the dart impacts.*

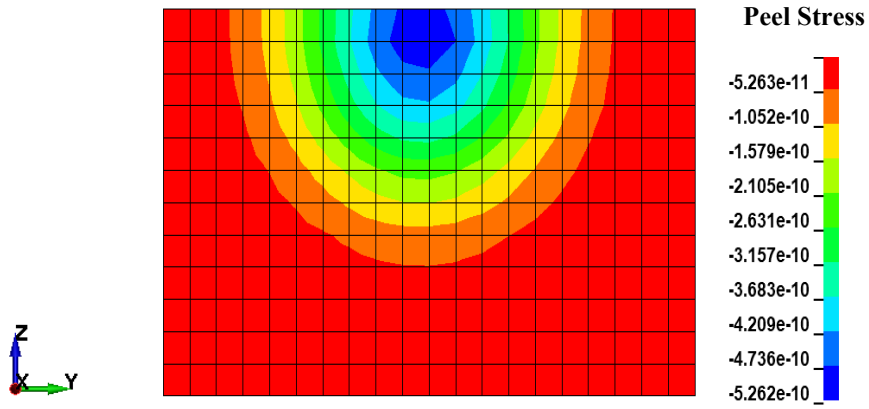

Figure 4.13 *Distribution of the peel stresses in the adhesive as the dart impacts.*

The shear stress is higher at the center of the layer and increases from top to bottom of the specimen. As it is shown in **figure 4.12** that just before failure of an adhesive layer, there are peel stress but an order of 10^{-2} MPa, which are very low, can be neglected, but these stresses are high in a single butt adhesive joint.

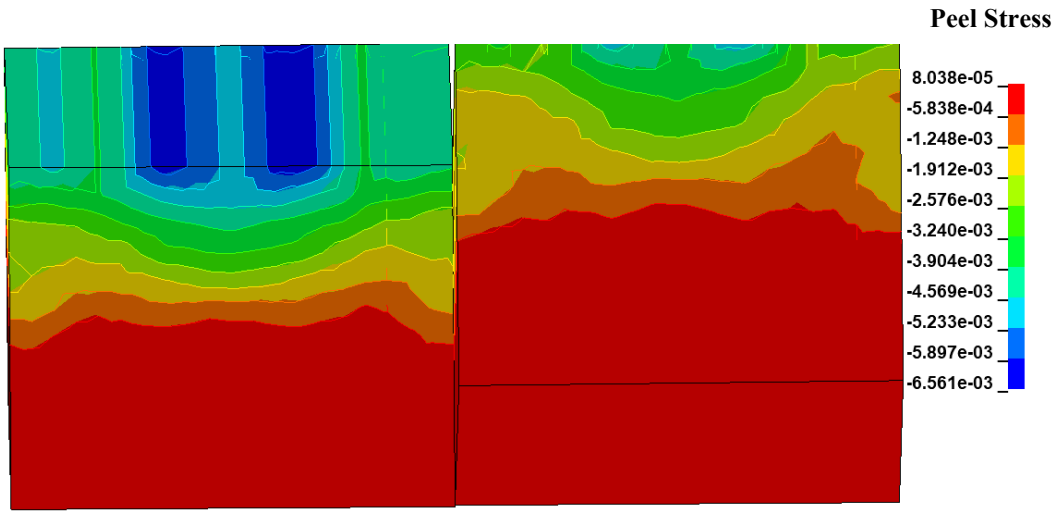

Figure 4.14 *Distribution of the peel stresses on the inner and outer side of adhesive just before the failure.*

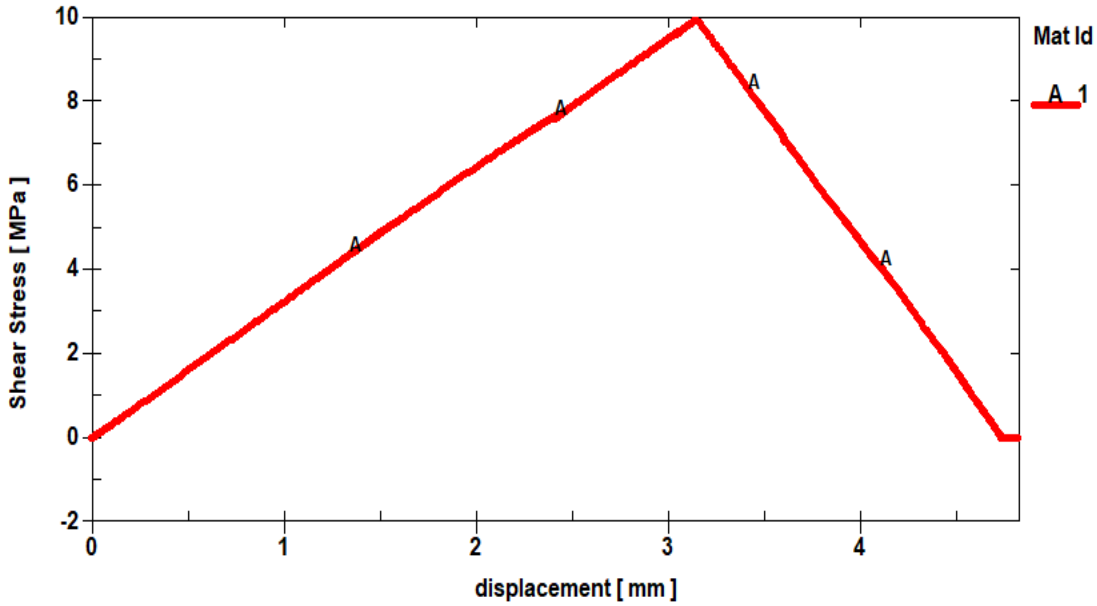

Figure 4.15 *Stress vs displacement of polyurethane adhesive*

The maximum value of the stress achieved during the simulation was 9.95 MPa if calculate the relative stress, i.e., the stress achieved divided by the shear strength (S) that we gave in the material model, it would be

$$Relative\ stress\ ratio = \frac{Maximum\ Stress\ obtained}{Shear\ Strength\ (S)} = \frac{9.95}{10} = 0.995$$

4.2.1.2 Energy Analysis

The energy absorbed under failure by the specimen is the essential data in an impact test. This is the critical information obtainable by experimental tests, not including auxiliary equipment. In this case, the numerical simulations were able to analyze the joint's behavior more intensely thanks to the solved stress and strain field during the computation. This work was used to obtain what part of dissipated energy is being absorbed by adhesive material that failed or consumed in the deformation of the adherends, and which parameters influence the results. It must be mentioned that being the one who studied a complete joint, the findings depend on both adhesive and substrate properties.

In the experimental drop dart test, this value is obtained by subsequent numerical integration of the force data recorded by the load cell. The total absorbed energy calculated in the numerical simulation resulted in being equal to the kinetic energy by the dart. The typical trend of the dart kinetic energy can be seen in **figure 4.14**. At the starting of simulation, the kinetic energy of the dart is constant, and it is a function of the impacting mass and the velocity of the dart $\left(E_K = \frac{1}{2}\, m\,.\,v^2\right)$. As soon as there is contact between dart and specimen, the dart velocity is slowly frayed as a function of contact force. The trend can be not very gradual because the contact with the impacting dart in Ls-Dyna is quite irregular, which may cause high peaks of force followed by the momentary loss of contact, which can also be seen in **figure 4.14** that the trend is not a straight line, but a slight curve form when there is loss of contact. At 0.7 ms, the failure occurs. The center substrate is detached, which cannot exploit any more resistance to the dart. The dart keeps moving down with its residual velocity and energy until the end of the simulation.

In the simulation, there are two more types energy that should be considered. One is frictional energy that is lost at the rigid walls on which adherends were placed. The coefficient of friction is defined on the surface of rigid walls and defined when there is a contact between dart and specimen value of the coefficient of friction was 0.3. And the other

one is due to hourglass energy, as was mentioned in **section 3.2.2.** The element formulation of type 1 is used to model the adherends because of the less computational power and the time. Its value is kept as small as possible, and in this work, it was always less than 0.08 J and can be considered negligible. The first essential result is that the energy absorbed by the adhesive accounts for most of the energy dissipated in the impact of the dart. Moreover, this quantity is all internal energy, i.e., strain energy. The value of 11.4 J is precisely the expected one known as the energy release rate of failure mode II of the epoxy adhesive: GIIC times the adhesive surface area for both the bonding regions.

$$E_{adhesive} = 2.(GIIC\,.width\,.thickness)$$

Impacting Energy (J)	Energy retained on the dart (J)	Absorbed Energy (J)
14	1.31	12.69

Table 4.1 *Energy division in case of the steel double butt epoxy joint*

Another positive outcome is that the adhesive material absorbs more than 89 % of the total absorbed energy, leaving the adherends a lower contribution than 10%, which is unquestionably good for a test on complete joints that identifies the properties of the adhesive material. This ratio may change with joint configuration and impacting energy.

Parameters	Energy (J)	$[\,E_i/E_a\,]$ %
$E_{absorbed}$	12.69	
$E_{adhesive}$	11.39	89.7 %
$E_{adherend}$	1.23	9.7 %
$E_{frict+Hg}$	0.07	0.6 %

Table 4.2 *Energy Analysis on the steel double butt joint*

The $E_{frict+Hg}$ is the summation of the energy dissipated in the friction and hourglass energy.

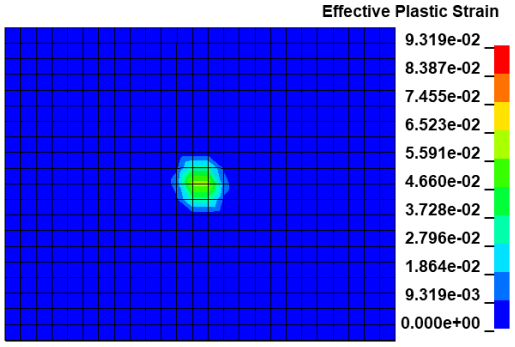

Figure 4.16 *Effective strain on the top surface of the middle adherend*

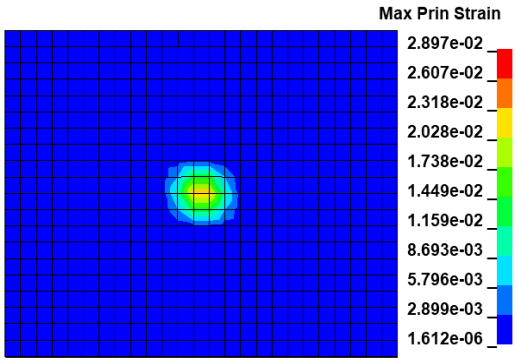

Figure 4.17 *Mean strain residual on the top surface of the middle adherend*

In **figures 4.16** and **4.17,** it was pretty evident that the middle adherend is deforming and absorbing some amount of the energy, i.e., energy analysis was done in table 4.2 was in matching with these results.

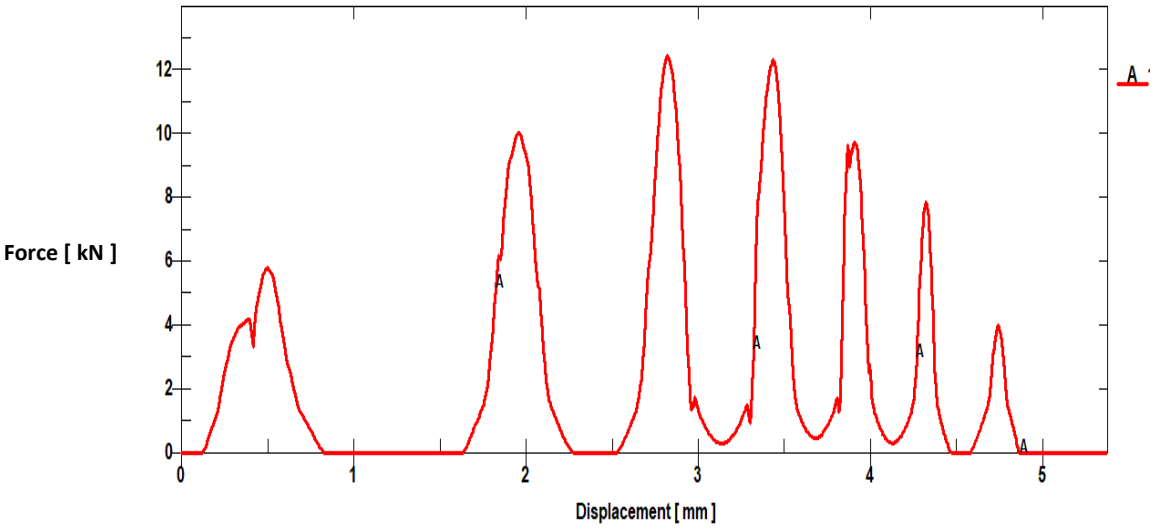

Figure 4.18 *Impacting force of dart on the middle adherend*

The force vs displacement plot obtained from the drop dart testing machine was not so smooth that it could be seen in **figure 4.18**; this is due to the detachment of the dart with the middle substrate as the kinetic energy of the middle substrate is more so, it moves down quicker than that of the dart. Some fluctuations can be filtere out by applying some low pass filter.

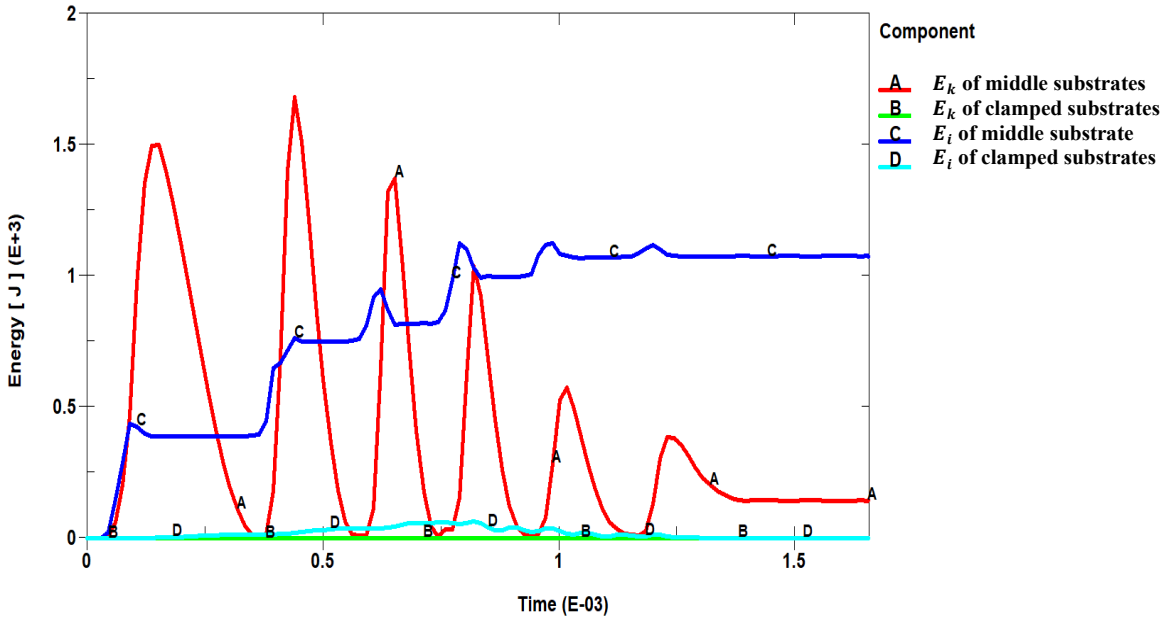

Figure 4.21 *Kinetic and the Internal Energy of the Clamped and the middle adherends*

As in figure 4.21, it can be seen that E_k of middle adherend is increasing to almost 1.6 J. Then it decreases because during the simulation it was observed that when there is no contact with the dart and the adherend the kinetic energy goes to zero and when the middle adherend is detached at 1.3 ms then the energy decreases to 0.2 J and never increases because the adhesive is failed.

4.2.1.3 Effect of dart velocity

In this portion, the effect of distinct impactor energy and velocity is examined. The analysis has been executed on the same model configuration with polyurethane adhesive discussed above. The adhesive and substrate material models both do not have any strain-rate-dependent material properties. However, some notable results have been figured out. Some

repetitive simulations have been done, keeping the impactor mass of 1 kg constant and gradually raising the velocity from a quasi-static test to the dart's impacting energy to be 18J. The quasi-static test has been completed with the same specimen configuration and the material model by assigning a prescribed motion to the impacting dart instead of defining an initial velocity. This constant velocity of the dart has been set to 1 mm/min. The data are summed up in **table 4.3**. It can be noticed that irrespective of the material model, which is not strain-rate dependent, the varying velocity of the impactor varies the absorbed energy of the joint, which can be observed in **figure 4.22**. This behavior is responsible for the dynamic effects: the higher the dart velocity is, the crueler or can say hasher the impact results would be. An increase in impactor velocity makes the duration of the test quicker, and the forces present in the system would be higher, causing a more significant deformation in the substrate and a more brutal indent that increasingly the strain energy of the substrate. This strain energy effect is primarily the function of the impacting energy.

Provided Energy [J]	18	16	14	Quasi-static
Absorbed energy [J]	13.3	12.96	12.69	10.42
E_i adhesive [J]	11.39	11.39	11.39	11.39
E_i adherend [J]	1.66	1.41	1.12	1.04
E_k adherend [J]	0.214	0.16	0.11	0

Table 4.3 *Effect on impactor energy.*

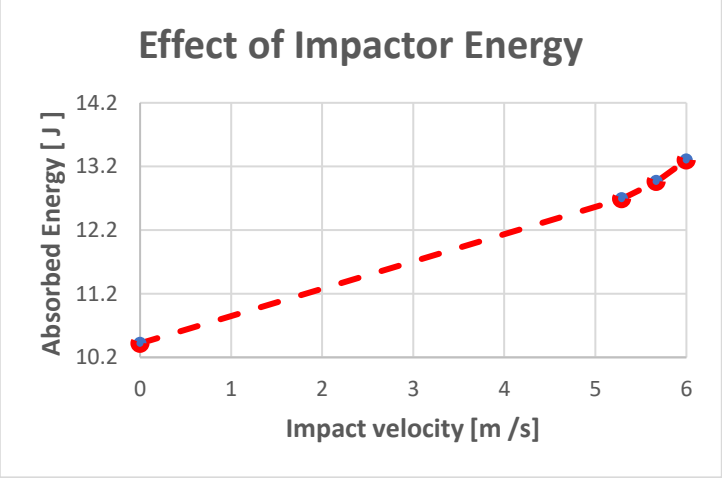

Figure 4.22 *Effect of dart velocity on absorbed energy. The value at null velocity is the quasi-static test.*

While on the other side, the energy absorbed by the adhesive is constant no matter what the dart velocity is, a direct effect of the failure of each cohesive element that precisely dissipates the material energy release rate, which is defined in the material model. The quasi-static results act as a lower limit of the absorbed energy, showing that a minimum of almost 10% of the absorbed energy is to be dissipated by adherends, in plastic deformation of them.

4.2.1.4 Effect of thickness

Another configuration is tested with the same amount of adhesive, i.e., the width of the specimen is 12 mm, and the thickness of the model is 20mm, as shown in figure 4.23.

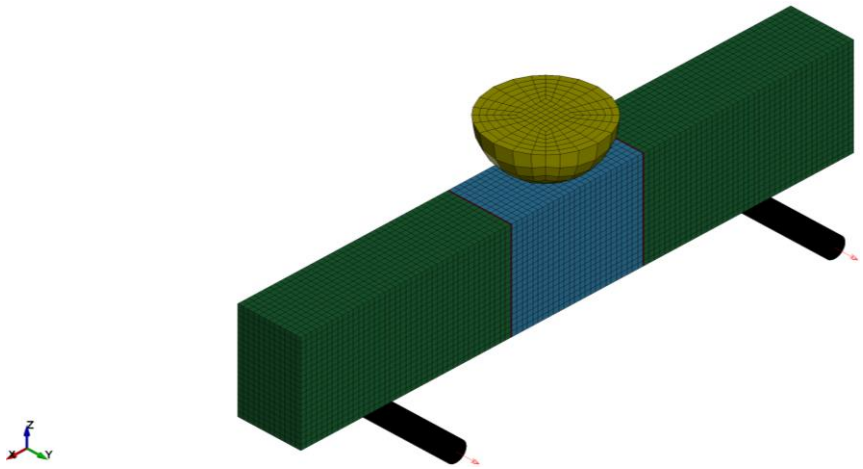

Figure 4.23 *Steel specimen with thickness 20 mm and width 12mm.*

The energy provided to the dart is the same as in the case mentioned earlier; the internal energy absorbed by the substrate is slightly different in case of less thickness. But the amount of energy absorbed by the adhesive is the same as the case mentioned earlier because the bonded specimen area is the same. Therefore, the type of failure is the same, i.e., mode II failure.

Parameters	Energy (J)	$[\ E_i/E_a\ ]\ \%$
$E_{absorbed}$	12.63	
$E_{adhesive}$	11.39	90.2 %
$E_{adherend}$	1.1	8.7 %
$E_{frict+Hg}$	0.14	1.1 %

4.2.2 Composite Substrate with Epoxy Adhesive

Parameters of the adhesive material are the following:

Adhesive width: 20 mm (along the y-direction)

The adhesive thickness on both sides: 0.2 mm;

Adhesive material: Epoxy

Parameters of the adherend material are the following:

Adherend width is the same as that of the adhesive, i.e., 20 mm

Adherend thickness: 7.04 mm with the 8 layers of fiber

Adherend material: carbon fiber twill weave pattern.

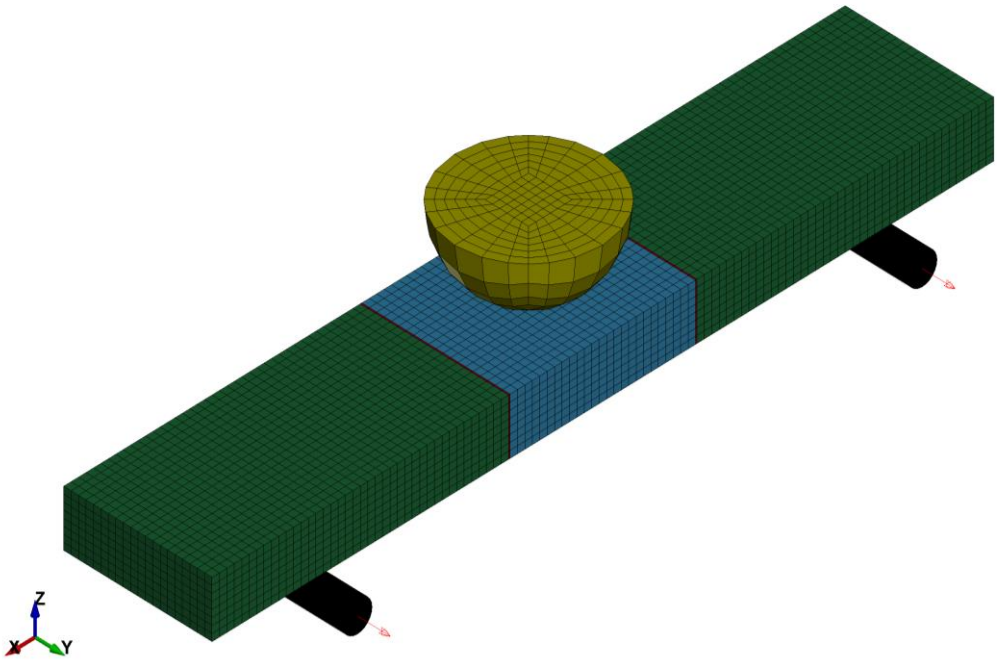

Figure 4.24 *Numerical model of the composite double butt joint with polyurethane adhesive*

The other dimensions that are mentioned in **section 4.2.1** are the same. However, as the thickness of the adherends is less than the one discussed in steel adherends, the amount of the adhesive material used is less in this case. Furthermore, the adhesive used is polyurethane, which is quite more flexible than the epoxy adhesive.

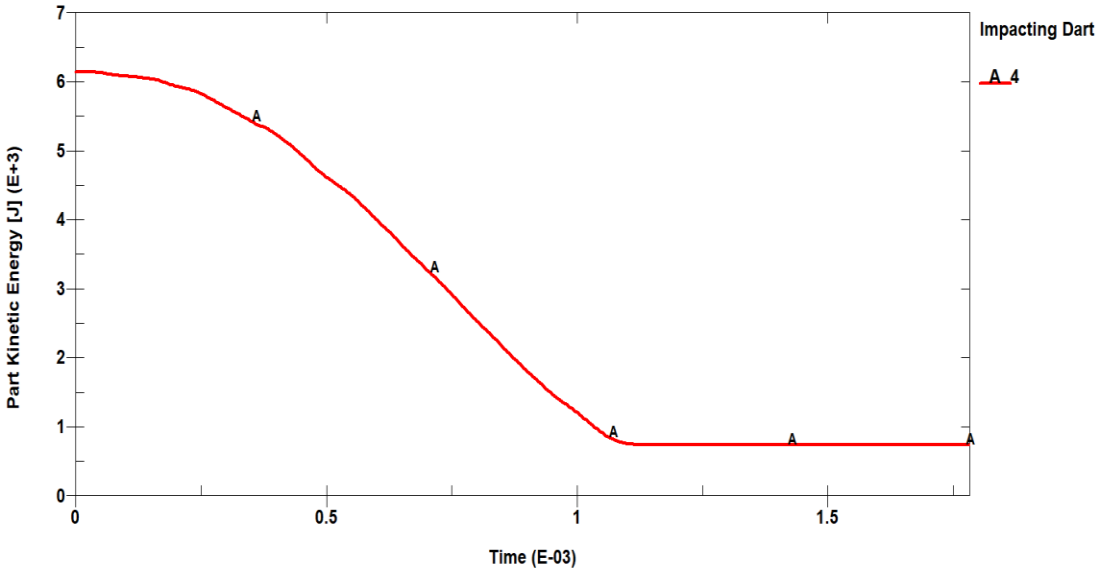

Figure 4.25 *Kinetic Energy of the Impacting Dart*

The mass of the dart was fixed as 1 kg, and the velocity was 3.5 m/s; as the dart moves down, kinetic energy is transferred to the specimen; after impact, the energy retained on the dart was 0.75J.

4.2.2.1 Stress Analysis:

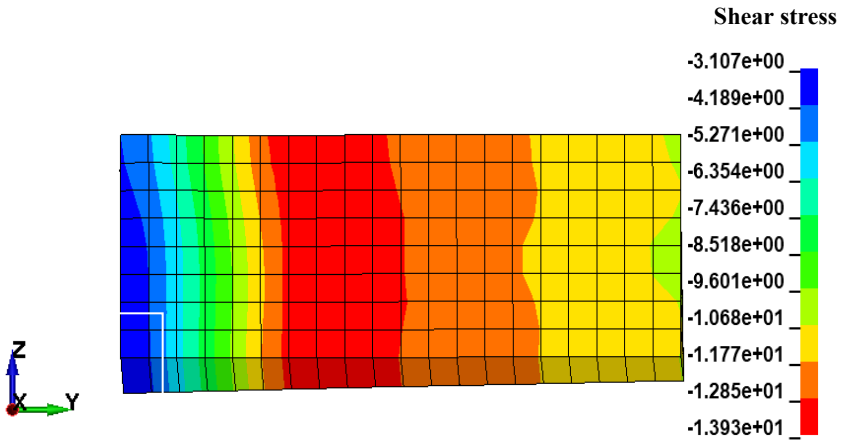

Figure 4.26 *Shear stress distribution just before the adhesive failure*

The red color represents the highest value of stress. The lowest one is the blue one, which is the order of 3.1 MPa; the value of the stress is with the negative sign, which means that the normal vector of an adhesive element is in the opposite direction.

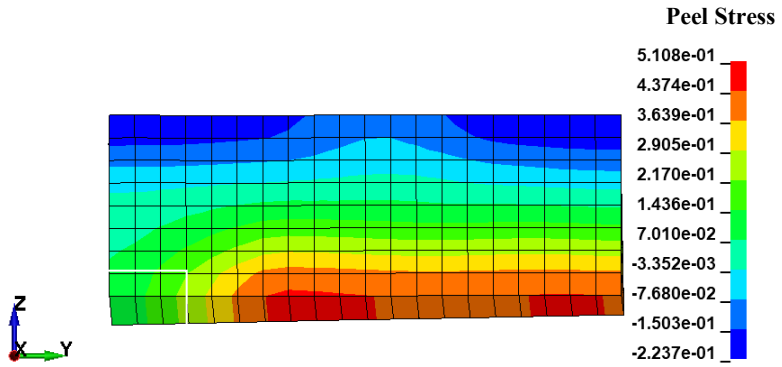

Figure 4.27 *Peel stress distribution just before the adhesive failure*

The maximum value of the peel stress just before the adhesive failure is 0.51 MPa. From **figure 4.27,** it is pretty evident that the model developed was quite good in the sense it is achieving its objective for what it is designed for, which means the adhesive is failing only in mode II (shear failure).

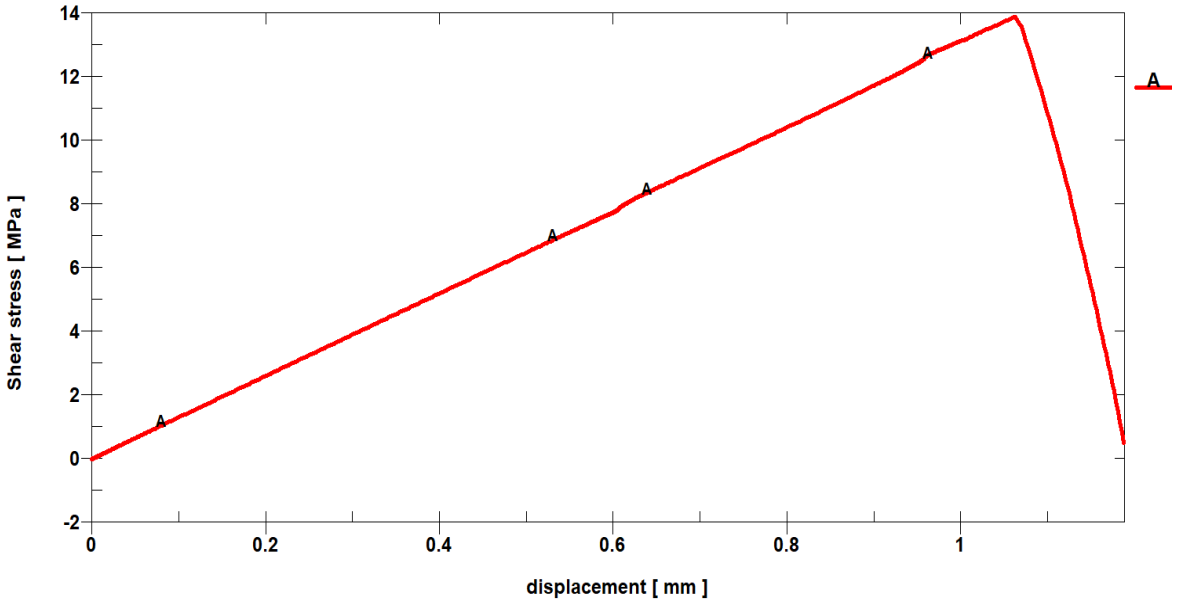

Figure 4.28 *Stress vs displacement of epoxy adhesive*

4.2.2.2 Energy Analysis

As this work is related to the impact properties of the adhesive material so, it is helpful to do the energy analysis on our system.

Impacting Energy (J)	Energy retained on the dart (J)	Absorbed Energy (J)
6.12	0.934	5.19

Table 4.4 *Energy division in case of the composite double butt epoxy joint*

Another positive outcome is that the adhesive material absorbs more than 78% of the total absorbed energy, leaving the adherends a lower contribution than 18%, which is unquestionably good for a test on complete joints that identify the properties of adhesive material. However, this ratio may change with joint configuration and impacting energy.

Parameters	Energy (J)	$[\ E_i/E_a\ ]\ \%$
$E_{absorbed}$	5.19	
$E_{adhesive}$	2.3	44.3 %
$E_{adherend}$	2.09	40.27 %
$E_{frict+Hg}$	0.8	15.43 %

Table 4.5 *Energy Analysis on the composite double butt joint*

The $E_{frict+Hg}$ is the summation of the energy dissipated in the friction and hourglass energy.

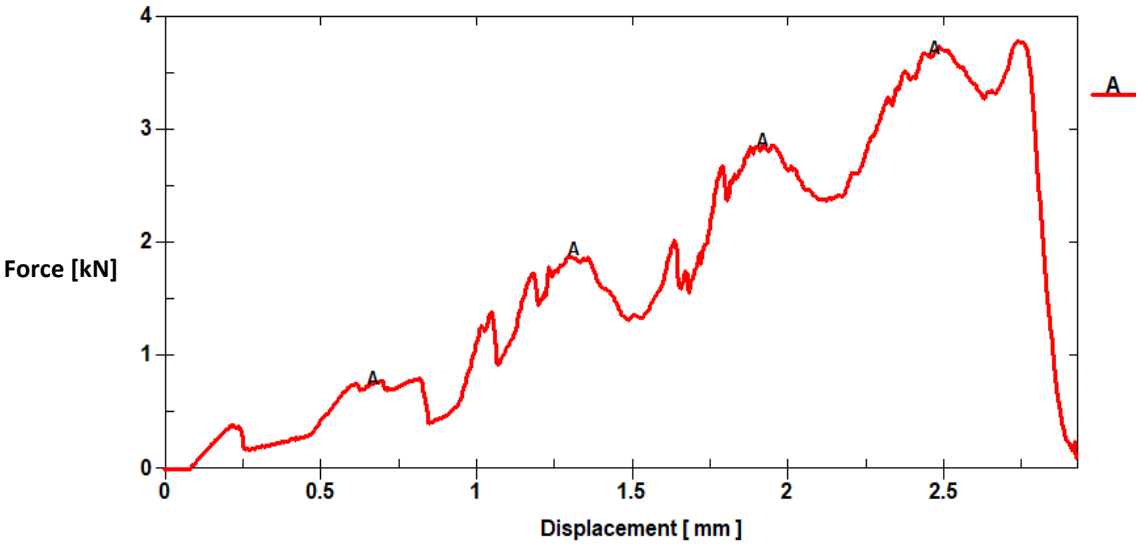

Figure 4.29 *Force vs displacement of the composite double butt joint*

The force absorbed by the composite material was reasonable, so there is no detachment of the dart with the middle adherend. The energy absorbed by the composite material was kinetic and internal, but the internal energy absorbed by the composite was more than that of the kinetic energy. As a result, there is no detachment of the specimen with the dart. Polyurethane adhesive is suitable for absorbing energy because the energy release rate used in the model was more than that of the epoxy adhesive

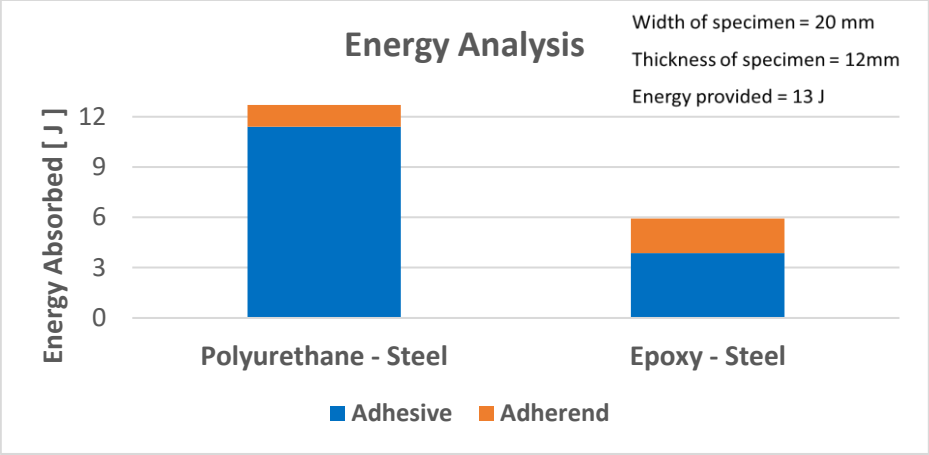

Figure 4.30 *Energy analysis of the steel double butt joint*

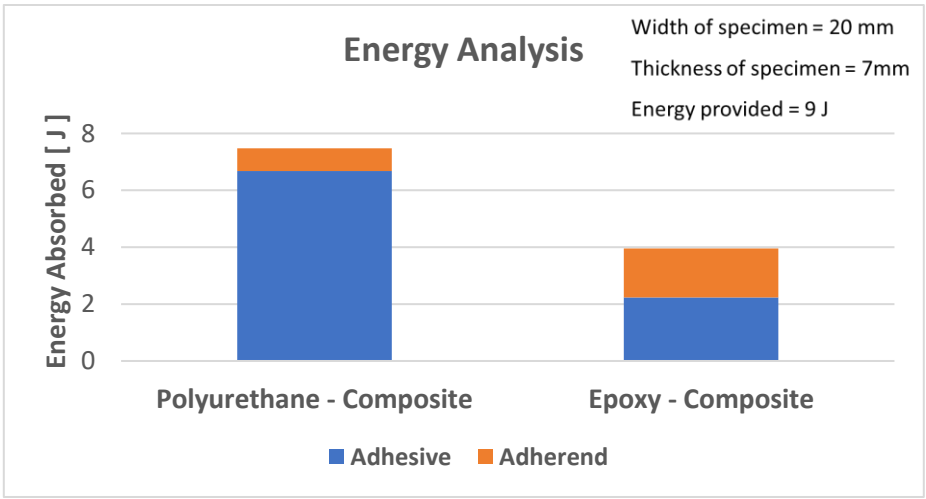

Figure 4.31 *Energy analysis of the composite double butt joint*

In both figures, it can be observed that a higher strength adhesive increases the adherend absorbs energy. And as the composite material are good in energy absorption, the energy absorbed by the composite substrates is more than that of the steel.

Chapter 5 Conclusion

A new methodology and model have been developed for the impact tests on adhesive joints in this work. Single butt joint and double butt joint have been designed to estimate the mechanical properties of adhesives in mode II (shear) under significant strain rate loading conditions. The parameterized joint geometry can be quickly adapted to a variety of materials. This methodology can be a beneficial tool in material research and exceptionally tune the material models utilized in finite element analysis. The model's different configuration has been devised and optimized through numerical modeling in Ls-Dyna. The numerical simulations able to exhibit the designed shear failure and the energy absorption capabilities of the joint have been analyzed. The simulations results demonstrated that the single butt joint is not an excellent option to obtain the shear properties of the adhesive joint since there is a problem of load eccentricity and some dynamic effects. And it requires a high velocity to test the single butt adhesive joint, which might not be possible for the drop dart machine to provide. So, there is quite a significant possibility of getting the mixed model failure instead of the mode II failure.

But as far the concern of the double butt joint is concerned, it exhibits pretty good results in terms of the shear failure, and there is very little probability of having the mode I failure or the mixed-mode failure. Some experimental tests in quasi-static loading conditions have been conducted on the single strap lap joints by the research group. These tests revealed the main problem of the clamping system. So, numerically the double butt joint is quite balanced, i.e., both adhesive layers are failing simultaneously. There is no problem with the load eccentricity. To evaluate the mechanical properties of the adhesive joint, not only adhesive and adherend materials are to be considered. But also the clamping system should be taken into consideration, as well as bonded materials, a simultaneous failure in both bonded regions is needed to occur. Several models are simulated with the one side of more clamped length than the other side, which illustrated that one bonded area failed and the other not. There are certain main future developments; one would be implementing the

continuum model approach to model the adhesive material to understand the crack initiation and its propagation correctly. And the other would be to conduct some dynamic tests that would evaluate the actual behavior of the model under a considerable strain rate, and a high-speed camera can be used to observe the crack propagation in the experimental test.

Appendix I

Butt joint created with Gmsh and Ls-Dyna

```
import gmshTools as gmsh
import numpy as np
from subprocess import call
import math

#geo parameters
SpecimenWidth = 20.0
AdherendLength1 = 25.0
AdherendLength2 = AdherendLength3 = 40.0 #mm
AdhesiveThick = AdherendThick1 = AdherendThick2 =Adherendthick3 = 7.04 #mm
AdhesiveLength = AdhesiveLength2 = 0.2 #mm
#Mesh parameters
mesh_reduce = 1 #mm
nn_x = np.int(AdhesiveLength/mesh_reduce + 2.0) #n of nodes in the adhesive
nn_y = np.int(SpecimenWidth/mesh_reduce + 1) #n of nodes in the y direction

####### Mesh the geometry and create  .k file for Adhesive1 element
x1 = 0
x2 = AdhesiveLength
with open('geo_solid_adhesive1.geo', 'w') as fout:                                  #create a new
file
   with open('geo_base_solid_adhesive.geo', 'r') as fin:                              #open the
settings .geo file
      for line in fin:                                                  #loop over the lines of fin
         line = line.replace('msize',
                        '{:>4.2f}'.format(mesh_reduce))       #assign mesh size
         line = line.replace('x1',
                        '{:>4.1f}'.format(x1))
         line = line.replace('x2',
                        '{:>4.1f}'.format(x2))
         line = line.replace('adhthick',
                        '{:>4.2f}'.format(AdhesiveThick))   #assign adhesive thickness
         line = line.replace('nn_x',
                        '{:>4d}'.format(nn_x))            #assign node in x direction
         line = line.replace('nn_y',
                        '{:>4d}'.format(nn_y))            #assign node in y direction
         fout.write(line)

GeoFile = "geo_solid_adhesive1.geo"
MeshFile = "geo_solid_adhesive1.inp"
gmshOptFile = "Mesh.opt"
```

```
call(r"C:\Program Files\gmsh-4.6.0-Windows64\gmsh " + gmshOptFile + " " + GeoFile + " -
3 -o " + MeshFile +
       " -format " + MeshFile[-3:], shell=False)
call('del *.pos', shell=True)

KFile = "elem_adhesive1.k"
gmsh.inp2k3D(MeshFile, KFile)
NNod_adhes = np.int(nn_x*nn_y*9)
NEl_adhes = np.int((nn_x-1)*(nn_y-1)*8)
```

####### Mesh the geometry and create .k file for Adhesive2 element

```
x1 = AdhesiveLength + AdherendLength1
x2 = AdhesiveLength + AdherendLength1 + AdhesiveLength2
with open('geo_solid_adhesive2.geo', 'w') as fout:                    #create a new
file
   with open('geo_base_solid_adhesive.geo', 'r') as fin:                    #open the
settings .geo file
      for line in fin:                                    #loop over the lines of fin
         line = line.replace('msize',
                     '{:>4.2f}'.format(mesh_reduce))      #assign mesh size
         line = line.replace('x1',
                     '{:>4.1f}'.format(x1))
         line = line.replace('x2',
                     '{:>4.1f}'.format(x2))
         line = line.replace('adhthick',
                     '{:>4.2f}'.format(AdhesiveThick))   #assign adhesive thickness
         line = line.replace('nn_x',
                     '{:>4d}'.format(nn_x))            #assign node in x direction
         line = line.replace('nn_y',
                     '{:>4d}'.format(nn_y))            #assign node in y direction
         fout.write(line)

GeoFile = "geo_solid_adhesive2.geo"
MeshFile = "geo_solid_adhesive2.inp"
gmshOptFile = "Mesh.opt"
call(r"C:\Program Files\gmsh-4.6.0-Windows64\gmsh " + gmshOptFile + " " + GeoFile + " -
3 -o " + MeshFile +
       " -format " + MeshFile[-3:], shell=False)
call('del *.pos', shell=True)

KFile = "elem_adhesive2.k"
gmsh.inp2k3D(MeshFile, KFile)
```

####### Mesh the geometry and create .k file for Adherend 1 elements

```
nn_x2 = np.int(AdherendLength1/mesh_reduce + 1) #n of nodes in the adherends
x2 = AdhesiveLength + AdherendLength1
x1 = AdhesiveLength
```

```
with open('geo_solid_adherend1.geo', 'w') as fout:                                  #create a
new file
   with open('geo_base_solid_adhesive.geo', 'r') as fin:                            #open the
settings .geo file
      for line in fin:                                                  #loop over the lines of fin
         line = line.replace('msize',
                        '{:>4.2f}'.format(mesh_reduce))       #assign mesh size
         line = line.replace('x1',
                        '{:>4.1f}'.format(x1))
         line = line.replace('x2',
                        '{:>4.1f}'.format(x2))
         line = line.replace('adhthick',
                        '{:>4.2f}'.format(AdhesiveThick))   #assign adhesive thickness
         line = line.replace('nn_x',
                        '{:>4d}'.format(nn_x2))             #assign node in x direction
         line = line.replace('nn_y',
                        '{:>4d}'.format(nn_y))             #assign node in y direction
         fout.write(line)

GeoFile = "geo_solid_adherend1.geo"
MeshFile = "geo_solid_adherend1.inp"
gmshOptFile = "Mesh.opt"
call(r"C:\Program Files\gmsh-4.6.0-Windows64\gmsh " + gmshOptFile + " " + GeoFile + " -
3 -o " + MeshFile +
       " -format " + MeshFile[-3:], shell=False)
call('del *.pos', shell=True)

KFile = "elem_adherend1.k"
gmsh.inp2k3D(MeshFile, KFile)

NNod_adher1 = np.int(nn_x2*nn_y*9)
NEl_adher1 = np.int((nn_x2-1)*(nn_y-1)*8)
```

####### Mesh the geometry and create .k file for Adherend 2 elements

```
nn_x2 = np.int(AdherendLength2/mesh_reduce + 1) #n of nodes in the adherends
x2 = 0
x1 = AdherendLength2
with open('geo_solid_adherend2.geo', 'w') as fout:                                  #create a
new file
   with open('geo_base_solid_adhesive.geo', 'r') as fin:                            #open the
settings .geo file
      for line in fin:                                                  #loop over the lines of fin
         line = line.replace('msize',
                        '{:>4.2f}'.format(mesh_reduce))       #assign mesh size
         line = line.replace('x1',
                        '{:>4.1f}'.format(-x1))
         line = line.replace('x2',
                        '{:>4.1f}'.format(x2))
```

```
        line = line.replace('adhthick',
                            '{:>4.2f}'.format(AdhesiveThick))   #assign adhesive thickness
        line = line.replace('nn_x',
                            '{:>4d}'.format(nn_x2))             #assign node in x direction
        line = line.replace('nn_y',
                            '{:>4d}'.format(nn_y))              #assign node in y direction
        fout.write(line)

GeoFile = "geo_solid_adherend2.geo"
MeshFile = "geo_solid_adherend2.inp"
gmshOptFile = "Mesh.opt"
call(r"C:\Program Files\gmsh-4.6.0-Windows64\gmsh " + gmshOptFile + " " + GeoFile + " -
3 -o " + MeshFile +
       " -format " + MeshFile[-3:], shell=False)
call('del *.pos', shell=True)

KFile = "elem_adherend2.k"
gmsh.inp2k3D(MeshFile, KFile)

NNod_adher23 = np.int(nn_x2*nn_y*9)
NEl_adher23 = np.int((nn_x2-1)*(nn_y-1)*8)

####### Mesh the geometry and create  .k file for Adherend 3 elements
x2 = AdhesiveLength + AdherendLength1 + AdhesiveLength2 + AdherendLength3
x1 = AdhesiveLength + AdherendLength1 + AdhesiveLength2
with open('geo_solid_adherend3.geo', 'w') as fout:                                  #create a
new file
   with open('geo_base_solid_adhesive.geo', 'r') as fin:                            #open the
settings .geo file
      for line in fin:                                          #loop over the lines of fin
         line = line.replace('msize',
                             '{:>4.2f}'.format(mesh_reduce))      #assign mesh size
         line = line.replace('x1',
                             '{:>4.1f}'.format(x1))
         line = line.replace('x2',
                             '{:>4.1f}'.format(x2))
         line = line.replace('adhthick',
                             '{:>4.2f}'.format(AdhesiveThick))   #assign adhesive thickness
         line = line.replace('nn_x',
                             '{:>4d}'.format(nn_x2))             #assign node in x direction
         line = line.replace('nn_y',
                             '{:>4d}'.format(nn_y))              #assign node in y direction
         fout.write(line)

GeoFile = "geo_solid_adherend3.geo"
MeshFile = "geo_solid_adherend3.inp"
gmshOptFile = "Mesh.opt"
```

```
call(r"C:\Program Files\gmsh-4.6.0-Windows64\gmsh " + gmshOptFile + " " + GeoFile + " -
3 -o " + MeshFile +
       " -format " + MeshFile[-3:], shell=False)
call('del *.pos', shell=True)

KFile = "elem_adherend3.k"
gmsh.inp2k3D(MeshFile, KFile)



####### Define parts in LS-DYNA
box1 = np.int(-AdherendLength2)
box2 = np.int(x2)
with open('double_butt_Impact_Test.k    ', 'w') as fout:                                    #create a
new file
   with open('double_butt_Impact_Test_base.k', 'r') as fin:                                #open the
settings .k file
      for line in fin:
         line = line.replace('boxxmin1',
                     '{:>8.1f}'.format(box1-1))
         line = line.replace('boxxmax1',
                     '{:>8.1f}'.format(box1+10))
         line = line.replace('boxxmin2',
                     '{:>8.1f}'.format(box2-10))
         line = line.replace('boxxmax2',
                     '{:>8.1f}'.format(box2+1))
         line = line.replace('idnodeoff1',
                      '{:>10.4f}'.format(NNod_adhes))
         line = line.replace('idelemoff1',
                      '{:>10.4f}'.format(NEl_adhes))
         line = line.replace('idnodeoff2',
                      '{:>10.4f}'.format(2*NNod_adhes))
         line = line.replace('idelemoff2',
                      '{:>10.4f}'.format(2*NEl_adhes))
         line = line.replace('idnodeoff3',
                      '{:>10.4f}'.format(2*NNod_adhes+NNod_adher1))
         line = line.replace('idelemoff3',
                      '{:>10.4f}'.format(2*NEl_adhes+NEl_adher1))
         line = line.replace('idnodeoff4',
                      '{:>10.4f}'.format(2*NNod_adhes + NNod_adher1 + NNod_adher23))
         line = line.replace('idelemoff4',
                      '{:>10.4f}'.format(2*NEl_adhes + NEl_adher1 + NEl_adher23))
         line = line.replace('idnodeoff5',
                      '{:>10.4f}'.format(2*NNod_adhes          +          NNod_adher1          +
2*NNod_adher23))
         line = line.replace('idelemoff5',
                      '{:>10.4f}'.format(2*NEl_adhes + NEl_adher1 + 2*NEl_adher23))
         fout.write(line)
```

Appendix II

Formulations for the failure criteria used for the type 59 material model. When any of the criteria below are true, the material is said to have failed in the corresponding mode.

1. Longitudinal tension ($\sigma_{11} > 0$)

$$\left(\frac{\sigma_{11}}{X_t}\right) + \left(\frac{\sigma_{12}}{S_{12}}\right) + \left(\frac{\sigma_{13}}{S_{13}}\right) \geq 1.$$

2. Transverse tension ($\sigma_{22} > 0$)

$$\left(\frac{\sigma_{22}}{X_t}\right) + \left(\frac{\sigma_{12}}{S_{12}}\right) + \left(\frac{\sigma_{23}}{S_{23}}\right) \geq 1.$$

3. Through-thickness shear (combined with long. Tension), ($\sigma_{11} > 0$)

$$\left(\frac{\sigma_{11}}{X_t}\right) + \left(\frac{\sigma_{13}}{S_{13}}\right) \geq 1.$$

4. Delamination (through-thickness tension)

$$\left(\frac{\sigma_{33}}{Z_t}\right) + \left(\frac{\sigma_{13}}{S_{12}}\right) + \left(\frac{\sigma_{23}}{S_{23}}\right) \geq 1.$$

where the first term is considered only if $\sigma_{33} > 0$

5. Through-thickness shear (combined with transverse tension), ($\sigma_{22} > 0$)

$$\left(\frac{\sigma_{22}}{Y_t}\right) + \left(\frac{\sigma_{23}}{S_{23}}\right) \geq 1.$$

6. Longitudinal compression

$$\left(\frac{\sigma_{11}}{X_C}\right) \geq 1$$

where $\sigma_{11} < 0$.

7. Transverse compression

$$\left(\frac{\sigma_{22}}{S_{12} + S_{23}}\right)^2 + \left[\left(\frac{Y_c}{S_{12} + S_{23}}\right)^2 - 1\right]\frac{\sigma_2}{|Y_c|} + \left(\frac{\sigma_{12}}{S_{12}}\right)^2 + \left(\frac{\sigma_{12}}{S_{12}}\right)^2 \geq 1$$

where the first term is considered only if $\sigma_{22} < 0$.

8. Through-thickness compression:

$$\left(\frac{\sigma_{33}}{S_{13} + S_{23}}\right)^2 + \left[\left(\frac{Z_c}{S_{13} + S_{23}}\right)^2 - 1\right]\frac{\sigma_2}{|Z_c|} + \left(\frac{\sigma_{13}}{S_{13}}\right)^2 + \left(\frac{\sigma_{23}}{S_{23}}\right)^2 \geq 1$$

where the first term is considered only if $\sigma_{33} < 0$.

References

[1] Welding, Brazing and Soldering, ASM International1993.

[2] Joining: Understanding the Basics, ASM International2011.

[3] P. Scallan, 4 - Material evaluation and process selection, in: P. Scallan (Ed.), Process Planning, Butterworth-Heinemann, Oxford, 2003, pp. 109-170.

[4] K. Sampath, Design for Joining, in: G.E. Dieter (Ed.), Materials Selection and Design, ASM International1997, p. 0.

[5] F.C. Campbell, Structural Joints—Bolted and Bonded, Structural Composite Materials, ASM International2010, p. 0.

[6] Chapter 1 - Introduction and Adhesion Theories, in: S. Ebnesajjad (Ed.), Adhesives Technology Handbook (Second Edition), William Andrew Publishing, Norwich, NY, 2009, pp. 1-19.

[7] M.P. Edward, Handbook of Adhesives and Sealants, Second Edition, 2nd ed. ed., McGraw-Hill Education, New York, 2007.

[8] S. Ebnesajjad, A.H. Landrock, Chapter 4 - Classification of Adhesives and Compounds, in: S. Ebnesajjad, A.H. Landrock (Eds.), Adhesives Technology Handbook (Third Edition), William Andrew Publishing, Boston, 2015, pp. 67-83.

[9] S. Ebnesajjad, A.H. Landrock, Chapter 1 - Introduction and Adhesion Theories, in: S. Ebnesajjad, A.H. Landrock (Eds.), Adhesives Technology Handbook (Third Edition), William Andrew Publishing, Boston, 2015, pp. 1-18.

[10] ASTM D5573-99(2019), Standard Practice for Classifying Failure Modes in Fiber-Reinforced-Plastic (FRP) Joints, ASTM International, West Conshohocken, PA, 2019.

[11] J. Shields, Adhesives Handbook, 1984.

[12] Adhesives — Determination of the mode 1 adhesive fracture energy of structural adhesive joints using double cantilever beam and tapered double cantilever beam specimens, INTERNATIONAL STANDARD, 2009, p. 24.

[13] ATM D3433 - 99(2020), Standard Test Method for Fracture Strength in Cleavage of Adhesives in Bonded Metal Joints, ASTM International, West Conshohocken, PA, 2020.

[14] F.J.P. Chaves, L.F.M. da Silva, M.F.S.F. de Moura, D.A. Dillard, V.H.C. Esteves, Fracture Mechanics Tests in Adhesively Bonded Joints: A Literature Review, The Journal of Adhesion 90(12) (2014) 955-992.

[15] B. Watson, C.-H. Liao, M.J. Worswick, D.S. Cronin, Mode I traction-separation measured using rigid double cantilever beam applied to structural adhesive, The Journal of Adhesion 96(8) (2020) 717-737.

[16] A. Khayer Dastjerdi, E. Tan, F. Barthelat, Direct Measurement of the Cohesive Law of Adhesives Using a Rigid Double Cantilever Beam Technique, Experimental Mechanics 53(9) (2013) 1763-1772.

[17] G. Cricrì, Cohesive law identification of adhesive layers subject to shear load The Twice Notched Flexure Test, Procedia Structural Integrity 12 (2018) 492-498.

[18] G. Kelly, Joining of Carbon Fibre Reinforced Plastics for Automotive Applications, Aeronautical and Vehicle Engineering, KTH Royal Institute of Technology, Stockholm, Sweden, 2004.

[19] A. Hrennikoff, Solution of Problems of Elasticity by the Framework Method, Journal of Applied Mechanics 8(4) (2021) A169-A175.

[20] Livermore software technology corporation (LSTC), LS-DYNA Keyword User's Manual Volume II-R8876, Livermore software technology corporation (LSTC), 2017.

[21] F. Armero, S. Oller, A general framework for continuum damage models. I. Infinitesimal plastic damage models in stress space, International Journal of Solids and Structures 37(48) (2000) 7409-7436.

[22] A.A. Bezemer, C.B. Guyt, A. Vlot, New impact specimen for adhesives: optimization of high-speed-loaded adhesive joints, International Journal of Adhesion and Adhesives 18(4) (1998) 255-260.

[23] B. Valès, S. Marguet, R. Créac'hcadec, L. Sohier, J.F. Ferrero, P. Navarro, An experimental method dedicated to the dynamic characterization of structural adhesives under drop weight conditions, International Journal of Adhesion and Adhesives 90 (2019) 106-125.

[24] L. Goglio, Impact Tests, in: L.F.M. da Silva, A. Öchsner, R.D. Adams (Eds.), Handbook of Adhesion Technology, Springer International Publishing, Cham, 2018, pp. 555-592.

[25] R.D. Adams, J.A. Harris, A critical assessment of the block impact test for measuring the impact strength of adhesive bonds, International Journal of Adhesion and Adhesives 16(2) (1996) 61-71.

[26] M. You, M.-B. Li, Y.-L. Yuan, G. Lin, F.-W. Ma, L.-F. Du, S.-J. Tang, Review of experimental techniques for impact property of adhesive bonds, International Journal of Adhesion and Adhesives 100 (2020) 102620.

[27] B.R.K. Blackman, A.J. Kinloch, A.C. Taylor, Y. Wang, The impact wedge-peel performance of structural adhesives, Journal of Materials Science 35(8) (2000) 1867-1884.

[28] ISO, Adhesives — Determination of dynamic resistance to cleavage of high-strength adhesive bonds under impact wedge conditions — Wedge impact method, 11343 2019.

[29] H.M.C. Ali Gursel, Adhesive Joints Subjected to Impact Loading: A Review, International Journal of Materials Engineering 2019, (2019) 6.

[30] T. Yokoyama, Experimental determination of impact tensile properties of adhesive butt joints with the split Hopkinson bar, 38(3) (2003) 233-245.

[31] L. Goglio, L. Peroni, M. Peroni, M. Rossetto, High strain-rate compression and tension behaviour of an epoxy bi-component adhesive, International Journal of Adhesion and Adhesives 28(7) (2008) 329-339.

[32] T. Yokoyama, K. Nakai, N.H. Mohd Yatim, High Strain-Rate Compressive Properties and Constitutive Modeling of Bulk Structural Adhesives, The Journal of Adhesion 88(4-6) (2012) 471-486.

[33] T. Yokoyama, K. Nakai, Determination of the impact tensile strength of structural adhesive butt joints with a modified split Hopkinson pressure bar, International Journal of Adhesion and Adhesives 56 (2015) 13-23.

[34] J. Neumayer, P. Kuhn, H. Koerber, R. Hinterhölzl, Experimental Determination of the Tensile and Shear Behaviour of Adhesives under Impact Loading, The Journal of Adhesion 92(7-9) (2016) 503-516.

[35] W.A. Lees, Toughened structural adhesives and their uses, International Journal of Adhesion and Adhesives 1(5) (1981) 241-247.

[36] A. Beevers, M.D. Ellis, Impact behaviour of bonded mild steel lap joints, International Journal of Adhesion and Adhesives 4(1) (1984) 13-16.

[37] M. Jordan, The instrumented guillotine impact testing apparatus, International Journal of Adhesion and Adhesives 8(1) (1988) 39-46.

[38] C. Sun, M.D. Thouless, A.M. Waas, J.A. Schroeder, P.D. Zavattieri, Ductile–brittle transitions in the fracture of plastically-deforming, adhesively-bonded structures. Part I: Experimental studies, International Journal of Solids and Structures 45(10) (2008) 3059-3073.

[39] S. Hayashida, T. Sugaya, S. Kuramoto, C. Sato, A. Mihara, T. Onuma, Impact strength of joints bonded with high-strength pressure-sensitive adhesive, International Journal of Adhesion and Adhesives 56 (2015) 61-72.

[40] J.J.M. Machado, P.M.R. Gamarra, E.A.S. Marques, L.F.M. da Silva, Numerical study of the behaviour of composite mixed adhesive joints under impact strength for the automotive industry, Composite Structures 185 (2018) 373-380.

[41] W. Cheng, J. Hallquist, Implementation of three-dimensional composite failure model into DYNA3D, Livermore Software Technol Corporation (2004).

[42] R. Ciardiello, C. Boursier Niutta, F. Di Sciullo, L. Goglio, Single-lap joints of similar and dissimilar adherends bonded with a polyurethane adhesive used in the automotive industry, IOP Conference Series: Materials Science and Engineering 1038(1) (2021) 012031.

[43] L.S.T.C. (LSTC), LS-DYNA KEYWORD USER'S MANUAL VOLUME I-R9023, LIVERMORE SOFTWARE TECHNOLOGY CORPORATION (LSTC), 2017.